A geometric morphometric approach to investigate primate proximal phalanx diaphysis shape.

Running title: **Phalangeal curvature shape**

Sophie E. Wennemann [1], Kristi L. Lewton [1, 2], Caley M. Orr [3, 4], Sergio Almécija [5, 6, 7], Matthew W. Tocheri [8, 9, 10], William L. Jungers [11, 12], Biren A. Patel [1, 2, *]

[1] Department of Integrative Anatomical Sciences, Keck School of Medicine, University of Southern California, Los Angeles, CA 90033, USA

[2] Human and Evolutionary Biology Section, Department of Biological Sciences, University of Southern California, Los Angeles, CA 90089, USA

[3] Department of Cell and Developmental Biology, University of Colorado School of Medicine, Aurora, CO 80045, USA

[4] Department of Anthropology, University of Colorado Denver, Denver, CO 80217, USA

[5] Division of Anthropology, American Museum of Natural History, Central Park West at 79th Street, New York, NY 10024, USA

[6] New York Consortium in Evolutionary Primatology, New York, NY, USA

[7] Institut Català de Paleontologia Miquel Crusafont, Universitat Autònoma de Barcelona, c/ Columnes s/n, Campus de la UAB, 08193, Cerdanyola del Vallès, Barcelona, Spain

[8] Department of Anthropology, Lakehead University, Thunder Bay, Ontario P7B 5E1, Canada

[9] Human Origins Program, National Museum of Natural History, Smithsonian Institution, Washington DC 20013, USA

[10] Australian Research Council Centre of Excellence for Australian Biodiversity and Heritage, University of Wollongong, Wollongong, New South Wales, 2522, Australia

[11] Department of Anatomical Sciences, Stony Brook University School of Medicine, Stony Brook, NY 11794, USA

[12] Association Vahatra, BP 3972, Antananarivo 101, Madagascar

* Corresponding author: Biren A. Patel, 1333 San Pablo Street, BMT 404, Keck School of Medicine, University of Southern California, Los Angeles CA, 90033, USA; Email address: birenpat@usc.edu

Keywords: phalanx; curvature; geometric morphometrics; included angle; suspensory

Funding Statement

Funding for this research was generously provided by: National Science Foundation (BCS #1317047 to B.A.P.; BCS #1539741 to C.M.O.); the L.S.B. Leakey Foundation (to B.A.P.); the Wenner-Gren Foundation (to C.M.O.); AEI/FEDER EU (CGL2017-82654-P to S.A.), Generalitat de Catalunya (CERCA Programme to S.A.); the University of Southern California's URAP program (to B.A.P.), and the University of Southern California's Office of the Provost (to S.E.W.).

Abstract

Current approaches to quantify phalangeal curvature assume that the long axis of the bone's diaphysis approximates the shape of a portion of a circle (included angle method) or a parabola (second-degree polynomial method). Here we developed, tested, and employed an alternative geometric morphometrics-based approach to quantify diaphysis shape of proximal phalanges in humans, apes and monkeys with diverse locomotor behaviors. 100 landmarks of the central longitudinal axis were extracted from 3D surface models and analyzed using 2DGM methods, including Generalized Procrustes Analyses. Principal components analyses were performed and PC1 scores (>80% of variation) represented the dorsopalmar shape of the bone's central longitudinal axis and separated taxa consistently and in accord with known locomotor behavioral profiles. The most suspensory taxa, including orangutans, hylobatids and spider monkeys, had significantly lower PC1 scores reflecting the greatest amounts of phalangeal curvature. In contrast, bipedal humans and the quadrupedal cercopithecoid monkeys sampled (baboons, proboscis monkeys) exhibited significantly higher PC1 scores reflecting flatter phalanges. African ape (gorillas, chimpanzees and bonobos) phalanges fell between these two extremes and were not significantly different from each other. PC1 scores were significantly correlated with both included angle and the *a* coefficient of a second-degree polynomial calculated from the

same landmark dataset, but had a significantly higher correlation with included angles. Our alternative approach for quantifying diaphysis shape of proximal phalanges to investigate dorsopalmar curvature is replicable and does not assume *a priori* either a circle or parabola model of shape, making it an attractive alternative compared with existing methodologies.

1. Introduction

The hand skeletons of living primates are morphologically diverse and reflect the unique evolutionary histories of various primate lineages as well as the ways that primates use their hands for manipulation and locomotion (e.g., Napier, 1993; Kivell et al., 2016). For example, proximal phalanges vary greatly within and among extant primate taxa in terms of how curved the shafts are (hereafter referred to as phalangeal curvature; Fig. 1). Highly suspensory primates (e.g., *Pongo*, *Hylobates, Symphalangus*, and *Ateles*) have very curved proximal phalanx shafts (i.e., high phalangeal curvatures), whereas habitually terrestrial pronograde species (e.g., *Gorilla* and *Papio*) along with bipeds (i.e., humans) have straighter shafts (i.e., low phalangeal curvatures) (e.g., Stern, Jungers & Susman, 1995; Dean & Begun, 2008; Rein, 2011). Primates that are more generalist in their substrate preference (e.g., *Pan* and *Macaca*) tend to have phalangeal curvature that is intermediate or more variable in grade compared with these two extremes (e.g., Jungers et al., 1997). These observed differences in phalangeal curvature are behaviorally linked to how primates use their hands when moving. Furthermore, theoretical models (Preuschoft, 1973b), along with both *in vitro* and *in silico* experimental biomechanical studies (Richmond, 2007; Nguyen et al., 2014) have shown that phalangeal curvature in primates is in large part an adaptation to the habitual mechanical loading environment that arises from substrate reaction forces, muscle forces from the contraction of extrinsic digital flexors, and joint reaction forces at the both the metacarpophalangeal and interphalangeal joints when the hands are used during locomotor and positional behaviors. Additionally, there is a phylogenetic component to phalangeal curvature variation among living primates which is likely a result of a long history of strong selection for attenuating these mechanical loads on relatively mechanically weak bones that are also important for manipulation in addition to locomotion (e.g., Wallace, Burgess & Patel, 2020; but see Richmond, 1998 and Jungers et al., 2002 for alternative hypotheses). Because of the strong form-function relationship between phalangeal curvature and locomotion in extant primates, paleoanthropologists typically use phalangeal curvature to infer

the positional and locomotor behavior of fossil primate species including hominins (Preuschoft, 1973a; Stern & Susman, 1983; Susman, Stern & Jungers, 1984; Hamrick, Meldrum & Simons, 1995; Susman, de Ruiter & Brain, 2001; Kivell et al., 2011, 2015; Domínguez-Rodrigo et al., 2015; Stratford et al., 2016; Prang et al., 2021).

Figure 1 Here

Different methods have been used to quantitatively assess phalangeal curvature in extant and fossil primates. The most prevalent approach has been to calculate the bone's included angle (IA), which assumes that the central longitudinal (i.e., proximodistal) axis of a phalanx represents a shape that corresponds to a portion of an arc on the perimeter of a circle (Fig. 2A; Stern, Jungers & Susman, 1995). Larger values of IA, measured in degrees, indicate bones that are more curved whereas smaller values indicate bones that are flatter. In general, this method does well to distinguish extant species based on habitual locomotor behavior, with the most suspensory primate species having larger IAs and more terrestrial species (both bipedal and pronograde quadrupedal) having smaller IAs (e.g., Rein, 2011). Despite the relatively high accuracy of this form-function relationship in extant primates, some authors (e.g., Patel & Maiolino, 2016) have noted that published IA values can differ substantially between studies (i.e., high inter-study variation). For example, IA mean (and one standard deviation) values reported for *Pan troglodytes* by Stern, Jungers & Susman (1995), Matarazzo (2008), and Rein (2011) are 42.4° (4.8°), 55.0° (4.4°) and 38.4° (5.3°), respectively. Even more variable are IA mean (and one standard deviation) values reported for *Macaca fascicularis*, where Matarazzo (2008), Rein (2011), and Patel & Maiolino (2016) reported values of 45.0° (6.6°), 16.2° (6.6°) and 22.0° (7.0°), respectively. With such a large amount of variation exhibited in IA values for a single species between studies, and researchers often being unable to independently collect IA data for a comparative sample or when describing new fossils (e.g., Stratford et al., 2016), it is unclear on which dataset researchers should rely, if any, when trying to make functional inferences about fossil specimens.

Figure 2 Here

Reasons for such inter-study discrepancies are unclear, but they could simply be related to different sample compositions (i.e., different museum collections). Alternatively, they could derive from the different tools used to acquire raw data such as handheld coordinate calipers (Susman, Stern & Jungers, 1984; Stern, Jungers & Susman, 1995), Microscribe point digitizers (Rein, 2011), three-dimensional (3D) landmarking software (Patel & Maiolino, 2016; Wallace, Burgess & Patel, 2020), or lateral view photographs (e.g., Richmond, 1998; Jungers et al., 2002; Burgess, 2018; Prang et al., 2021). In fact, some of these tools might be more prone to error than others. For example, there can be movement artifacts when applying a Microscribe point digitizer on small specimens (B.A.P. personal observation) and photographs can suffer from parallax issues if the specimen is not positioned properly relative to the lens of the camera (Spencer & Spencer, 1995; Richmond, 1998). Another overlooked problem of lateral view photographs of proximal phalanges is that important morphological features needed to calculate IA of the central longitudinal axis can be obscured in the field of view (Fig. 1). One example of this is the presence of well-developed flexor sheath ridges (as found in *Gorilla*) that can incorrectly inflate measurements of midshaft dorsopalmar height thus resulting in smaller calculated IA values (see equations and figures in Stern, Jungers & Susman, 1995; Jungers et al., 1997). In fact, low values of IA for *Gorilla* calculated from lateral view photographs often overlap extensively with human IA values (e.g., Prang et al., 2021), which would not be predicted based on biomechanical differences in hand use during locomotion between humans and gorillas. Another example is the presence of a very concave proximal articular surface (as seen in many monkeys like *Papio* that have a large range of dorsiflexion at the metacarpophalangeal joint) that when not fully visible can lead to erroneous longer proximodistal interarticular length measurements resulting in larger IAs. Hence, it is important to acknowledge that end users (e.g., paleoanthropologists) relying on published IA data for comparisons with fossil phalanges should proceed with caution (e.g., always use a single source of comparative data and follow its same methodology for taking measurements) or should only use original self-collected data.

Some researchers have argued against using IAs for assessing phalangeal curvature claiming that it may be theoretically flawed. Specifically, Deane, Kremer & Begun (2005) argued that the diaphyses of primate proximal phalanges, in particular the dorsal surfaces, look

more like parabolas or a second-degree (2°) polynomial[1] rather than portions of a circle and emphasized that the IA is an inappropriate metric to quantify phalangeal curvature (but see contrary arguments made by Stern, Jungers & Susman, 1995). A strong visual case for this opinion can be made by looking at the mid-sagittal plane of a proximal phalanx from taxa that have relatively straight bones like cercopithecine monkeys (e.g., *Papio* and *Nasalis*) and humans (Fig. 1). Accordingly, Deane, Kremer & Begun (2005) devised a High-Resolution Polynomial Curve Fitting method (hereafter referred to as PCF) that uses a lateral view photograph of a proximal phalanx to fit a second-degree polynomial function (defined as $y=ax^2+bx+c$) to an extensive number of two-dimensional (2D) landmarks placed on the dorsal surface of the diaphysis (Fig. 2B). The resulting *a* coefficient (or quadratic coefficient) is then used as a proxy metric for curvature where a larger *a* value is equivalent to a narrower parabola and signifies a more curved bone. In general, this method can distinguish extant species based on habitual locomotor behavior, with suspensory orangutans having larger *a* values and bipedal humans having smaller values for *a* (Deane, Kremer & Begun, 2005; Deane & Begun, 2008). A second argument subsequently made by Deane & Begun (2008) against using IA was that it has limited paleoanthropological utility because a large number of fossil phalanges are broken and only complete bones can be used to calculate IA correctly. These authors suggested that a benefit of using PCF is that it allows for the inclusion of more fossils in comparative analyses than would be possible if using IA alone. Although the use of this method has not been widespread in paleoanthropological research, it has recently been applied in studies of early hominin and Miocene hominoid fossil hand bones (Kivell et al., 2011, 2015; Böhme et al., 2019) (Fig. 2C).

Despite the reasonable arguments against implementing the IA method, however, it continues to be used (e.g., Stratford et al., 2016; Wallace, Burgess & Patel, 2020; Prang et al., 2021), most likely because the PCF method also has some practical disadvantages. The first is that as currently implemented PCF measures the curvature of the dorsal surface of the bone (Deane, Kremer & Begun, 2005) rather than the more biomechanically relevant central longitudinal axis that better reflects overall adaptation for attenuating mechanical stresses experienced by the bone during grasping (Preuschoft, 1973b; Richmond, 2007; Nguyen et al.,

[1] Note that the merits of a second-degree polynomial specifically for proximal phalanges over some other higher order polynomial function, such as third-sixth-degree, are discussed in detail by Deane, Kremer & Begun (2005) and are not repeated here. See also Zhang, Harrison & Ji (2020) who discuss the merits of a fourth-degree polynomial compared to a second-degree polynomial for proximal phalangeal curvature.

2014). Second, more taxonomically inclusive studies using PCF have shown inconsistent results regarding known form-function relationships in extant primates. Most notably, gibbons, which are among the most suspensory living primates, have a mean and range of *a* values that indicate a degree of curvature that is equal to some generalized arboreal quadrupedal monkeys (e.g., *Cercopithecus* and *Alouatta*) and overlap terrestrial quadrupedal knuckle-walking African apes (*Gorilla* and *Pan*) (Böhme et al., 2019).

In light of these issues with using both IA and PCF, the current study investigates the suitability of an alternative method to assess diaphysis shape of primate proximal phalanges. Specifically, we implemented geometric morphometrics (GM) methods to determine bone shape that is both biomechanically informative and reflects the dorsopalmar curvature of the central longitudinal (proximodistal) phalangeal axis. The use of GM to assess shape reflective of diaphysis curvature is not new and has been applied to other postcranial elements such as the femur, clavicle, and ulna (De Groote, Lockwood & Aiello, 2010; Squyres & DeLeon, 2015; Milne & Granatosky, 2021). In the current study, our alternative approach uses 3D digital surface models of proximal phalanges on which a semi-automated software workflow with minimal user input is applied to obtain landmarks that can be subjected to established GM methods. The utility of this GM approach is then assessed by comparing 2D shape by means of Principal Components (PC) scores among different extant anthropoid species with known locomotor behaviors. Finally, resulting PC scores reflecting diaphysis dorsopalmar curve shape are compared with curvature assessed from the same landmark datasets using the IA and PCF methods.

2. Materials and Methods

2.1 Comparative Sample

The comparative sample of 378 manual proximal phalanges of the third digit (mPP3) used in this study includes modern humans, chimpanzees, bonobos, gorillas, orangutans, siamangs, gibbons, baboons, proboscis monkeys, and spider monkeys (Table 1). Phalanges from digits 2, 4, and 5 (mPP2, mPP4, and mPP5) were also studied for a smaller subset of these primates (see below). These taxa were chosen because their habitual locomotor behaviors are relatively well known and have been quantified by primate behaviorists. Moreover, they represent taxa that engage in differing amounts of suspensory and quadrupedal locomotion, as

well as differing preferences for arboreal and terrestrial substrates (e.g., Rein [2011] and Granatosky [2018] and references therein). All specimens except for one gorilla and one spider monkey were collected in the wild based on museum records. The sample includes females and males as well as some where the sex is unknown; all of these were combined to maximize intraspecific variation, and to make the final datasets more applicable for future broader paleoanthropological studies. Most specimens were skeletal adults and had fully fused proximal epiphyses; a handful of non-human subadult specimens for some taxa were included if the epiphysis was in the process of fusion and could not be manually separated from the diaphysis (see Supplemental Information and Figure S1 for additional considerations on adult vs. subadult sampling). The studied specimens derive from the following collections: AMNH, American Museum of Natural History (New York, NY, USA); ANSP, Academy of Natural Sciences of Drexel University (Philadelphia, PA, USA); LACM, Natural History Museum of Los Angeles County (Los Angeles, CA, USA); MCZ, Harvard University Museum of Comparative Zoology (Cambridge, MA, USA); RMCA, Royal Museum for Central Africa (Tervuren, Belgium); SBU, Department of Anatomical Sciences of Stony Brook University (Stony Brook, NY, USA); USC, Department of Integrative Anatomical Sciences of the Keck School of Medicine of the University of Southern California (Los Angeles, CA, USA); USNM, Smithsonian Institution's National Museum of Natural History (Washington, DC, USA); WITS, University of the Witwatersrand (Johannesburg, South Africa), and the Mountain Gorilla Skeletal Project (MGSP). Additional details of the comparative sample are found in Table 1.

Table 1 Here

2.2 Surface Data

3D surface models of mPP3s were generated from computed tomography scans (CT), micro-CT scans (μCT), or laser surface scans following protocols detailed elsewhere (see Fernandez et al., 2015; Patel et al., 2017; Fig. 1). A number of studies have previously shown that different scanning modalities has little to no effect on most morphometric results (e.g., Tocheri et al., 2011; Robinson & Terhune, 2017; Shearer at et al., 2017). CT scans were obtained with slice intervals up to 0.187 mm (with scanning field of views that produced near isotropic voxels). μCT scans were obtained with isometric voxel dimensions up to 0.080 mm. The CT and

243 µCT scan data were segmented on unfiltered 16-bit *DICOM* (.dcm) or *TIFF* (.tif) images using
244 the SEGMENTATION EDITOR in Amira v.5.6 (or later) software (Thermo Fisher Scientific) by
245 means of a combination of automated and slice-by-slice manual thresholding techniques, after
246 which triangular surface meshes were created using the SURFACE GEN [or GENERATE SURFACE in
247 more recent versions of Amira] function (with 'unconstrained smoothing' and 'compactify'
248 options implemented) and saved as *POLYGON* mesh files (.ply). All laser scans were obtained
249 with a NextEngine 3D laser scanner (NextEngine, Inc.) using a resolution of >10,000 points per
250 square inch; 6 to 12 scans were taken at different positions and then merged using ScanStudio
251 HD PRO software (NextEngine, Inc.) and saved as .ply files.
252 The analytical procedures developed and employed in this study can potentially be
253 sensitive to the quality of the 3D surface meshes used. Therefore, any scanning defects (e.g.,
254 spikes, floating triangles, holes) in the mesh surface models created from any of the scanning
255 modalities were corrected using Geomagic Wrap software (3D Systems, Inc.). Additionally, any
256 biological holes (i.e., foramina) in the diaphysis from nutrient arteries were also virtually
257 removed. Each surface mesh was then made hollow to include only an external watertight shell
258 of triangles, which was then either decimated or refined to the same approximate size of 250,000
259 triangles (see Supplemental Information and Figure S2 for additional considerations about
260 preferred surface mesh triangle counts). All subsequent procedures and data acquisition were
261 performed on right side proximal phalanges; if the original specimen was from the left side, it
262 was first mirror-imaged in Amira or Geomagic Wrap to create an antimere.
263
264 *2.3 Landmark Data Acquisition*
265 The data acquisition methodology developed and used in this study relied on Amira and
266 ImageJ software (Schneider, Rasband & Eliceire, 2012); therefore, the terminology used here
267 reflects these software packages only. When possible, we provide names of specific functions,
268 modules, and plugins for each program that we implemented so that other users who prefer
269 different software (e.g., Avizo, Meshlab, MATLAB, Python, R, etc.) can replicate these methods
270 in the software package of their choice.
271 It was necessary to first position all surface models in the same anatomical orientation to
272 acquire equivalent landmarks from near the center of the diaphysis of a phalanx (Fig. 3A).
273 Rather than using previously published computational routines that facilitate automated

alignment of 3D surfaces (e.g., Boyer et al., 2015), we opted for a manual approach using a standardized protocol in Amira such that: 1) a line connecting the centers of the proximal and distal articular surfaces in dorsal view (XZ) was aligned vertically; 2) the palmar-most aspect of the proximal palmar tubercles and the palmar-most aspect of the distal trochlea in lateral view (YZ) were aligned on the same plane and positioned vertically; and 3) the palmar-most aspect of the proximal palmar tubercles in proximal view (XY) were aligned on the same plane and positioned horizontally. The initial orientation of specimens was facilitated using the ALIGN PRINCIPAL AXES module (which aligns the virtual bone according to its three principal axes; Axis 1 was set to 'x' and Axis 2 was set to 'y'), and this was followed by minor manual movements (facilitated by a checkerboard background) using the TRANSFORM EDITOR function (see below for error analyses for intra-observer differences in determining a standardized anatomical orientation). We refer to this as our 'gold standard' orientation from here forward.

Figure 3 Here

The gold standard orientation allows for subsequent re-slicing of the virtual phalanx to ultimately obtain cross sections that are oriented orthogonal to its long (proximodistal) axis. To re-slice a surface mesh of triangles, the mesh must first be converted to a volumetric representation with user defined voxel dimensions. This was accomplished using the SCAN CONVERT SURFACE (or SCAN SURFACE TO VOLUME in more recent versions of Amira) module, a tool that voxelizes (i.e., 3D pixilation) the surface mesh resulting in a binary label field (i.e., set of slices) of known dimensions. To create a new binary label field with enough resolution, we used a z-pixel dimension of 1000 while keeping the model's original x- and y-pixel dimensions unchanged (thereby yielding non-isotropic voxels in the resulting volume representation). For our purposes, this procedure effectively creates 1000 new binary image slices from proximal to distal ends of the bone which can be further cropped and further resampled (as discussed below) (Fig. 3B).

Because our goals are to identify shape reflecting dorsopalmar curvature of the most biomechanically relevant region of the diaphysis (i.e., non-articular regions), a new region of interest of the diaphysis (dROI) was defined between the palmar-most aspect of the proximal palmar tubercles and the inflection point between the distal trochlea and the diaphysis on the

palmar side (Fig. 3C; see Supplemental Information and Figure S1 for further discussion on dROIs of subadults with partial fusion of the proximal articular surfaces). The region proximal to the palmar tubercles and the entire distal trochlea was then cropped out using the CROPEDITOR function from the binary label field thereby resulting in a new image stack with less than 1000 slices. Due to differences in absolute phalangeal length as well as the size and shape of the trochlea and proximal ends among and within primate species (Fig. 1; see also Patel & Maiolino, 2016), the cropped binary label field was further resampled so that each specimen in the analysis yielded the same number of binary images; this step could not simply be implemented simultaneously with the previous one because of technical limitations in Amira. This second phase in resampling was accomplished by first generating a new 3D surface (using the SURFACE GEN function with the default 'add border' option not implemented), and then again using the SCAN CONVERT SURFACE function to voxelize and resample with a z-pixel dimension of 100 while again keeping the model's original x- and y-pixel dimensions unchanged. The new binary image stack of 100 cross section images was then saved in .tif format. Note that outputting a stack of 100 TIFF images within Amira also produces an important accompanying metadata file (".info") that contains real world dimensions (in mm) for pixel size (x and y) and slice position (z) from proximal to distal for the resulting set of images. This resolution information is needed after raw landmark coordinates are obtained to keep proper scaling of the raw data in real world units (see below).

The new stack of 100 binary images, each representing a cross section from proximal to distal of the reoriented phalanx's dROI, was then imported into ImageJ in order to find the cross-section's approximate center (Fig. 3D). While a number of approaches are possible to accomplish this, we chose a method that allows for both automation and replication with no user input, and an approach that we inferred to allow us to identify the approximate center between the dorsal and palmar surfaces of all slices independently. Specifically, we applied a modified looped version of the MAX INSCRIBED CIRCLES plugin written by Burri & Guiet (2016) and available from the PTBIOP Update Site for ImageJ, which implements the largest inscribed circle algorithm following code initially written by Birdal (2021) in MATLAB software (MathWorks). The looped plugin runs sequentially through the stack of 100 dROI cross sections finding a specific circle-shaped region of interest in each image, from which the x- and y-coordinates of their centers can be calculated using the CENTER OF MASS measurement function

in ImageJ (Fig. 3D). Using the known pixel resolution and slice spacing information from the .info file outputted from Amira (see above), these center x-, y-, and z-coordinates are then scaled back into real world dimensions (in mm). These 100 semi-landmarks are then subjected to geometric morphometric analyses.

2.4 Geometric Morphometrics

Phalanges have rather complex shapes with varying amounts of shaft torsion, flexor sheath ridge development, and general mediolateral asymmetry (Patel & Maiolino, 2016; see also Figs. 1 and 3D). Therefore, the position of a cross section's center can vary in the mediolateral (x-) direction when taking these features into account, whereas the dorsopalmar (y-) position of the center changes negligibly (i.e., less noisy). Accordingly, while the resulting output of the previous steps produced 3D landmarks, we chose to pursue a 2D geometric morphometric (2DGM) analysis since our primary concern is determining the dorsopalmar longitudinal shape of the phalanx's diaphysis (i.e., its dROI). Moreover, using a 2DGM approach also has the added benefit of being able to combine samples of right and left side bones, which is particularly useful when studying fragmentary fossil assemblages, or when reliable side determinations of isolated phalanges cannot be made by the researcher.

Landmark data files for each specimen exported from Amira consisted of y- and z-coordinates (i.e., dorsopalmar and proximodistal coordinates, respectively). These landmark data files were first manually configured to *Morphologika* format to facilitate import into R software (R Core Team, 2019) for analysis using the GEOMORPH package (Adams, Collyer & Kaliontzopoulou, 2019). Raw landmark configurations were scaled, translated, and rotated using Generalized Procrustes Analysis (GPA), which produced a new set of coordinates (Procrustes coordinates) that were then used for subsequent statistical analyses. A number of intra- and inter-observer error analyses were first performed using Procrustes distances resulting from the GPAs. Principal component analyses (PCA) were then performed to assess variance in shape via resulting principal component (PC) scores. It was determined that the first two PCs typically accounted for >80% of the variation in all of the 2DGM analyses implemented. Moreover, PC1 accounted for nearly all the shape variation of the phalanx's central longitudinal dorsopalmar curvature (see Figure S3) and thus we placed our primary emphasis on these values in the results of subsequent analytical tests of utility and comparability. All statistical analyses discussed in the

following paragraphs were performed in R software, JMP v.14 software (SAS Institute), or PAST software (Hammer, Harper & Ryan, 2001). The R script as implemented for all analyses is available in the Supplemental Information. Landmark data files in *Morphologika* format for the comparative sample of humans, apes, and monkeys are available on the journal's website.

3. Results and Discussion

3.1 Error

To assess the effects of intra- and inter-observer error, we performed three analyses. The first analysis for intra-observer error focused specifically on the specimen orientation protocol. The second analysis for intra- and inter-observer error examined the specimen dROI determination protocol. The final analysis for both intra- and inter-observer error evaluated all steps of the protocol.

3.1.1 Specimen orientation: To systematically investigate the effect of differences in specimen orientation in a realistic way, one observer (S.E.W.) performed a controlled sensitivity analysis in which one orangutan specimen (*Pongo abelii* AMNH-143598) was used to create 60 model variants that deviated 10 degrees (in 1 degree increments) from our gold standard model in six possible directions about this specimen's centroid: dorsal, palmar, medial, lateral, clockwise, counterclockwise (see insert in Fig. 4). We then performed all the landmark acquisition and 2DGM procedures outlined above on these model variants without altering any other parameters or inputs. Procrustes distances between the gold standard specimen and the 60 model variants were plotted against change in degrees in reference to the gold standard specimen to visually assess any relationship between model orientation and diaphysis shape (Fig. 4). Procrustes distances appear to differ inconsequentially when the specimen moved between 1 and 10 degrees from the gold standard in medial, lateral, clockwise, and counterclockwise directions. In contrast, Procrustes distances increased almost linearly when the oriented bone was incorrectly positioned in the dorsal and palmar directions from 1 to 10 degrees. Based on these findings, we emphasize the importance to orient specimens carefully prior to subsequent steps for landmark acquisition, especially in the dorsal and palmar directions about the bone's centroid.

Figure 4 Here

3.1.2 Specimen dROI determination: The cropping procedure to determine specimen dROI is also subject to both intra- and inter-observer error. Therefore, we performed an error study to test for both in which two observers (S.E.W. and B.A.P.) took one orangutan specimen (*Pongo abelii* AMNH-143598) and performed the cropping steps described above 10 times over a period of several days. We then performed all the landmark acquisition procedures outlined above without altering any other parameters or inputs. A 2DGM analysis was then performed on the resulting 20 landmark datasets (i.e., 10 landmark set replicates from two different observers), along with 16 additional *Pongo abelii* specimens (for a total n=36 individuals in the analysis; the latter 16 were quantified only by S.E.W.). The additional 16 *Pongo abelii* specimens were included to compare variation in Procrustes distances within each observer's and among the two observers' replicates (n=45 and n=100 comparisons, respectively), and to determine how these compare to variation in Procrustes distances between other specimens of the same species (n=136 comparisons). Box-and-whiskers plots (Fig. 5) demonstrate that intra- and inter-observer Procrustes distances for the test specimen (*Pongo abelii* AMNH-143598) are significantly smaller than the Procrustes distances among all specimens of *Pongo abelii*.[2] These findings indicate that any minor differences in cropping within and between observers is fundamentally negligible in larger scale comparisons within taxa (Fig. 5) and among taxa (see below).

Figure 5 Here

3.1.3 Complete protocol: Intra- and inter-observer error for the entire protocol was evaluated by two observers (S.E.W. and B.A.P.) using one orangutan specimen (*Pongo abelii* AMNH-143598). Both observers obtained the necessary landmark datasets 10 times over a period of one month. A 2DGM analysis was then performed on the resulting 20 landmark datasets (i.e., 10 landmark set replicates from two different observers), along with 16 additional *Pongo abelii* specimens (for a total n=36 individuals in the analysis; the latter 16 were quantified only by S.E.W.). As noted above, the additional 16 *Pongo abelii* specimens were included to compare variation in Procrustes distances within each observer's and among the two observers'

[2] Post-hoc analyses show that variation between and among observers was not significant ($p>0.05$) but was significant ($p<0.05$) when compared to total species variation.

replicates (n=45 and n=100 comparisons, respectively), and to determine how these compare to variation in Procrustes distances between other specimens of the same species (n=136 comparisons). Box-and-whiskers plots (Fig. 6) demonstrate that intra- and inter-observer Procrustes distances for the test specimen (*Pongo abelii* AMNH-143598) are significantly smaller than the Procrustes distances among all specimens of *Pongo abelii*.[3] Thus, these findings indicate that any minor differences in executing the entire protocol within and between observers is minimal in larger scale comparisons within taxa (Fig. 6) and among taxa (see below).

Figure 6 Here

3.2 *Inter-digit variation*

Because an ultimate objective for implementing this method is to evaluate shape of primate fossil phalanges, and not all primate fossil hands have a mPP3 preserved, we performed an analysis examining inter-digit variation by comparing diaphysis dorsopalmar shape across non-pollical proximal phalanges (i.e., mPP2–5). Specifically, we compared the mPP2-5s within a sample of orangutans (*Pongo abelii*; n=10) that have very curved proximal phalanges and within a sample of humans (*Homo sapiens*; n=12) that have straighter proximal phalanges (Fig. 1; Rein, 2011). The two samples were analyzed separately (i.e., subjected to their own 2DGM analyses) rather than being combined so that their resulting PC1 scores would not be influenced by the presence of different taxa with different levels of curvature. For each taxonomic sample, a non-parametric Kruskal-Wallis test and non-parametric Mann-Whitney pairwise comparisons were used to compare digit PC1 scores for the entirety of each species. In addition, we compared PC1 scores by individual (i.e., matched pairs: mPP2 vs. mPP3, mPP2 vs. mPP4, etc.) within each species sample using non-parametric Wilcoxon Signed Rank tests. Despite some dissimilarities across digits, there were no significant differences ($p>0.05$) in any of the comparisons in either species (Fig. 7). These results are consistent with findings reported for both IA and PCF methods that also observed no significant differences in phalangeal curvature across hand digits in both hominoid and cercopithecoid primates (Stern, Jungers & Susman, 1995; Deane & Begun 2008). More importantly, and for practical purposes, the lack of significant differences among digits

[3] Post-hoc analyses show that variation between and among observers was not significant ($p>0.05$) but was significant ($p<0.05$) when compared to total species variation.

(when analyzed among individuals or analyzed within an individual) suggests that if necessary, non-pollical proximal phalanges can be combined to increase sample sizes so that the 2DGM methods presented in this study can be employed more broadly. This is particularly useful when studying isolated fossil phalanges that may not necessarily come from the same digit as an existing comparative sample (e.g., from digit 3 as emphasized in this study).

Figure 7 Here

3.3 Utility

The utility of any novel quantitative method needs to be assessed and we would interpret our method to be useful if the PCAs resulted in group separations along known locomotor behaviors (i.e., with a shape morphocline from most curved to least curved corresponding to most suspensory/arboreal to least suspensory/arboreal and most terrestrial). Therefore, we performed a comprehensive 2DGM analysis on the entire comparative sample of 378 mPP3s of humans, apes, and monkeys (Table 1). The resulting PC scores were visualized using both bivariate scatter plots and box-and-whiskers plots, and interspecific statistical difference was assessed using ANOVA and post-hoc Tukey's tests for pairwise comparisons. We predicted that the more suspensory orangutans, gibbons, siamangs, and spider monkeys would plot near each other on a given PC score distribution, thereby reflecting proximal phalanges with greater curvature. In contrast, we predicted that humans and baboons would plot near each other on the same PC score distribution reflecting proximal phalanges with less curvature. Finally, we predicted that chimpanzees would be closer to the suspensory taxa (i.e., with more curved shape) whereas gorillas and proboscis monkeys would be closer to the non-suspensory taxa (i.e., less curved shape) of the resulting PC score distributions. In addition to comparing PC scores, species average diaphysis shapes based on Procrustes coordinates were visualized and compared to the sample mean shape.

The first two principal components accounted for ~92% of the total observed variation (85.3% for PC1 and 6.6% for PC2). Variation along PC1 tracks degree of suspensory behavior: highly suspensory primates were found on the negative side of the PC1 distribution and demonstrate more curved shapes, bipedal humans and pronograde quadrupedal monkeys were found on the positive side of the PC1 distribution and demonstrate flatter shapes, and African

apes were in the middle (Figs. 8 & 10; the mean, maximum and minimum shapes for PC1 and PC2 resulting from the 2DGM analysis are illustrated in Figure S3). ANOVAs reveal that there are significant differences in PC1 scores (F=123.00; df=12,365; p<0.0001) among the studied taxa (Fig. 9). Post-hoc analyses (Table 2) of PC1 scores also reveal the following: both *Pongo* species are significantly different from each other and from all other primates; hylobatids and *Ateles* do not differ from each other; African apes differ from all other primates examined but not each other; humans and *Nasalis* are not significantly different from each other; *Papio* is significantly different from all other primates except *Nasalis*.

To investigate the potential effects of variation in size on shape differences among taxa, we subsequently calculated the correlation between species mean PC1 scores and the natural log (ln) of dROI length (which was computed from the most proximal [#1] and distal [#100] landmarks). While this correlation was significant (r=-0.607; p=0.028), further review reveals that three groups, *Pongo abelii* and *Pongo pygmaeus* with absolutely the longest dROIs and *Papio* spp. with absolutely the shortest dROIs were the primary influencers driving significance in this analysis (see Figure S4A). When these three taxa are removed, and the correlation is performed again (see Figure S4B), it is found to be not significant (r=0.163, p=0.653). Thus, the latter demonstrates that species with similar mPP3 dROI lengths can exhibit quite different PC1 scores and therefore levels of phalangeal curvature, further supporting the general hypothesis that differences in mPP3 curvature shape relate to locomotor behavior.

ANOVA reveals that there are significant differences among taxa in PC2 scores (F=61.13; df=12,365; p<0.0001, Fig. 9). Post-hoc analyses of PC2 scores also reveal the following: all three *Gorilla* species have significantly higher PC2 scores than all other taxa; the smaller bodied hylobatids, *Ateles*, *Papio* and *Nasalis* have significantly lower PC2 scores, but do not generally differ among each other; humans do not differ from either species of *Pongo* or *Pan*.

Figure 8 Here

Figure 9 Here

Figure 10 Here

Table 2 Here

The 2DGM method to quantify proximal phalanx diaphysis shape produces results that

reflect dorsopalmar curvature and correspond with variation in known locomotor behaviors among the studied primate taxa. Hence, this novel alternative approach will be useful for future functional morphology studies. The results also show patterns of morphological variation that are generally consistent, but not exactly the same, with other methods (but see below for additional comparisons with IA and PCF). Despite the relatively intuitive pattern in species mean shape differences revealed by the PCA (Figs. 8-10) from more suspensory orangutans on one end of the spectrum of curvature shape variation to terrestrial quadrupedal baboons on the other, there were a few surprising results that did not match predictions, and which will require further inquiry. Specifically, the following five unexpected patterns were found: African apes do not significantly differ from each other in PC1 scores; the two species of orangutans are significantly different from each other in their PC1 scores; *Ateles* which uses forelimb suspension and quadrupedalism does not significantly differ from brachiating hylobatids; the two quadrupedal monkeys (*Papio* and *Nasalis*) rather than bipedal humans have the flattest phalangeal curve shapes; and all three gorilla taxa differ in their PC2 scores from all other primates studied here.

Because chimpanzees, bonobos, and gorillas all have similar diaphysis shapes to each other, and because they are significantly flatter in shape compared to the more habitually suspensory taxa, the dorsopalmar curvature observed here in the African apes does not necessarily reflect a suspensory adaptation alone or the significant differences in proportion of time spent suspensory behaviors (see Carlson [2005] and referenced therein). What is more likely is that their intermediate levels of curvature (as reflected by PC1 scores) better represents adaptations for more diverse hand postures used in arboreal behaviors more generally, such as vertical climbing, and may also reflect adaptations for quadrupedal locomotion with a knuckle-walking hand posture, among others (e.g., Tuttle, 1970l Thompson et al., 2018). This possibility is further supported by the fact that the quadrupedal cercopithecoid monkeys that use palmigrade and digitigrade hand postures (e.g., Patel, 2010, and references therein) and are not stereotypical orthograde vertical climbers have even flatter shapes than African apes. The large overlap among the African apes (i.e., no significant differences among genera or species), however, may further indicate that their phalangeal shapes may be due more to the lack of significant differences in the proportion of time spent vertical climbing and its associated hand kinematics (e.g., Neufuss et al., 2017), rather than the dramatic kinematic differences in knuckle-walking postures used among African apes (e.g., Tuttle, 1970; Matarazzo, 2013).

549 Sumatran orangutans (*Pongo abelii*) were found to have diaphysis shapes that are more
550 curved than Bornean orangutans (*Pongo pygmaeus*) (Figs. 9 and 10). Although previous studies
551 have not demonstrated differences in phalangeal curvature between orangutan species, this may
552 be because these studies either only included one orangutan species (e.g., Jungers et al., 1997;
553 Dean & Begun, 2008; Rein, 2011), or both species may have been combined into a more general
554 orangutan sample (e.g., Stern, Jungers & Susman, 1995). While the biological significance of
555 this difference in phalangeal curvature between orangutan species is uncertain, it may be related
556 to their different ecologies. Specifically, the Borneo orangutans (males in particular) frequent the
557 ground as part of their normal behaviors (Ancrenaz et al., 2014), whereas Sumatran orangutans
558 may use terrestrial substrates less frequently due to the presence of tigers on the island of
559 Sumatra (there are no known tigers on the island of Borneo as they likely have gone extinct;
560 Delgado & van Schaik, 2000). Thus, if the Bornean orangutan has had a longer recent
561 evolutionary history of descending to the ground compared to Sumatran orangutans, it may have
562 secondarily evolved flatter proximal phalanges (assuming high phalangeal curvature is ancestral
563 for the genus *Pongo*).
564 Among the monkeys studied here, spider monkeys (*Ateles*) are the only species that
565 habitually use forelimb suspensory locomotion and postural behaviors (e.g., Rein, 2011). Thus, it
566 is not surprising that *Ateles* phalanges are similar in diaphysis shape to those of gibbons and
567 siamangs (Figs. 9 and 10). Furthermore, considering that they do not significantly differ from
568 either hylobatid group, it confirms that suspensory behaviors have a greater influence on
569 increasing proximal phalangeal curvature than does a more generalized arboreal locomotor
570 repertoire (e.g., as seen in *Nasalis*). In contrast, the diaphysis shapes seen in *Nasalis* (an above-
571 branch arboreal quadruped) and *Papio* (a primarily terrestrial quadruped) are similar to each
572 other in this study and both represent the flattest phalangeal curvatures (of the taxa studied here).
573 It is not entirely clear why these two large bodied monkeys have similar shapes despite
574 differences in preferred substrates and quadrupedal hand postures (i.e., palmigrade for *Nasalis*
575 vs. digitigrade for *Papio*; Patel, 2010), but it may be possible that these levels of proximal
576 phalangeal curvatures are common to all cercopithecoids or simply because they do not engage
577 in any significant amount of suspensory locomotion. It is also equally likely that the curvature of
578 proximal phalanges is not sensitive enough for selection to act on subtle locomotor differences
579 among habitually pronograde quadrupeds like cercopithecoids, regardless of their degree of

arboreality. Additional cercopithecoid taxa that use some form of suspensory locomotion (e.g., *Pygathrix nameus*; Byron and Covert, 2004) should be included in future analyses to assess this possibility further. It is important to note that the similarity between *Papio* and *Nasalis* seen here does contrasts previous studies using IA (e.g., Jungers et al., 1997) and PCF (Deane and Begun, 2008) where both found *Papio* to have significantly flatter proximal phalanges than *Nasalis*. Again, the addition of more data from monkeys is needed to better understand this outcome.

The fact that both cercopithecoids included here also overlap with diaphysis shapes exhibited by bipedal humans (which rarely use their hands for locomotion) was unanticipated (Fig. 9). A number of plausible, but not mutually exclusive, reasons may account for this overlap. First, there is enough fossil evidence demonstrating that the earliest hominins had greater phalangeal curvature than modern humans thereby making it a primitive feature for the group (e.g., Stern & Susman, 1983; Tocheri et al., 2008; Kivell et al., 2011; Stratford et al., 2016; Prang et al., 2021). Thus, modern humans may simply have retained some degree of phalangeal curvature from more ancestral hominin species that were adapted for arboreality. Likewise, there may have been continued selection for moderate levels of phalangeal curvature throughout human evolution as an adaptation to attenuate higher mechanical loads while using powerful grips with large forces during stone tool production and use (e.g., Tocheri et al., 2008; Harmand et al., 2015). Further studies of curvature shape of fossil proximal phalanges from the Miocene, Pliocene and Pleistocene are needed to test these hypotheses further (e.g., Deane & Begin, 2008; Stratford et al., 2016). Alternatively, it may be that the large cercopithecoid monkeys (like *Papio* and *Nasalis*) have evolved to have flatter phalanges because their terrestrial or above branch arboreal quadrupedal locomotion, respectively, may not benefit from greater curvature (i.e., different mechanical loading regimes compared to below branch or vertical climbing locomotion). Quadrupedal monkeys of varying size, especially in the smaller body mass range, and substrate preference are needed to test this hypothesis further.

Finally, all three *Gorilla* taxa separated on PC2 in the full taxonomic analysis of diaphysis shape (Fig. 9). Upon closer inspection of the maximum and minimum shapes relative to the mean shape on PC2 (see Figure S3), and species mean shape relative to the sample mean shape (Fig. 10), it appears that gorillas differ from the other primates studied here in the location of the dROI's curvature main inflection point. For gorillas with higher PC2 scores, the curvature

611 inflection point appears to be slightly distal to the midpoint whereas in other taxa it is closer to
612 the midpoint or slightly more proximal. It is difficult to say why the dROI curvature inflection
613 point would differ between gorillas and other primates, but we do not think this is related to
614 habitual locomotor behavior, substrate preference, or even body size of these great apes.
615 Moreover, since PC2 accounts for ~6% of the total variation, it is unclear how, if at all,
616 biologically and biomechanically meaningful the unusual gorilla pattern really is. But this may
617 warrant further consideration in the future especially if it successfully separates African ape
618 genera (*Gorilla* vs. *Pan*) from each other.
619
620 *3.4 Comparability*
621 The primary motivation for this project was to find an alternative to both IA and PCF
622 methods to quantify proximal phalangeal curvature based on 3D morphology of the bone's
623 longitudinal central axis. One way to assess comparability between the different methods is with
624 correlation analyses. Here we correlated PC1 scores from the 2DGM analysis of the entire
625 comparative sample of 378 specimens with each specimen's IA and PCF *a* coefficient.
626 Specifically, both IA and *a* were calculated in Excel software (Microsoft) from the same set of
627 100 2D landmarks identified from the dROI used in the 2DGM shape analysis (see Figure S5).
628 Three of the landmarks – proximal [#1], middle [#50], and distal [#100] – were used to compute
629 IA following modified equations presented in Jungers et al. (1997). Note that IAs calculated
630 from our landmark data will not yield the same IAs as those obtained in other studies based on
631 different protocols (Stern, Jungers & Susman, 1995; Matarazzo, 2008; Rein, 2011) and thus
632 should not be directly compared. All 100 landmarks were used to fit a second-degree polynomial
633 in order to determine the *a* coefficient following Deane, Kremer & Begun (2005). One important
634 difference between Deane, Kremer & Begun's (2005) study and the present one is that the
635 second-degree polynomial was applied to the dorsal surface of the phalanx's diaphysis in the
636 former study whereas the second-degree polynomial was applied to the bone's longitudinal
637 central axis in the present study (compare Figure 2B with Figure S5). Pearson correlations were
638 assessed for two whole-sample comparisons: PC1 vs. IA and PC1 vs. *a*. Both correlations were
639 significant ($p<0.05$), but the r value for the correlation between PC1 and IA (r=-0.940; Fig. 11)
640 was much higher than that for the correlation between PC1 and *a* (r=-0.753; Fig. 12).
641 These results demonstrate that the 2DGM approach presented here to quantify diaphysis

642 shape of proximal phalanges reflecting longitudinal dorsopalmar curvature produces results that
643 are more in line with measures of included angle (and thus a portion of a circle) as championed
644 by Stern, Susman & Jungers (1995) rather than a second-degree polynomial (and hence a
645 parabola) as proposed by Deane, Kremer & Begun (2005). Despite the higher correlation, it is
646 particularly important to emphasize that our assessment of curvature shape in PC scores is not
647 the same as IA and thus does not specifically reflect a portion of a circle. In fact, the approach
648 presented here using 2DGM is not based on any *a priori* shape for phalangeal curvature. In
649 comparing PC1 scores, IA values, and *a* coefficients for each specimen by taxon (see Figure S6),
650 it is clear that the PC1 scores from the 2DGM analysis and IA values yield better results in
651 differentiating extant taxa by their habitual locomotor modes, whereas the *a* coefficient primarily
652 works well to discriminate only highly suspensory primates (i.e., *Pongo*, hylobatids, and *Ateles*)
653 from all others. That is to say, using the *a* coefficient derived from PCF as implemented in this
654 study does a relatively poorer job distinguishing among habitually arboreal and terrestrial
655 quadrupeds, as well as bipedal humans. We therefore recommend not using PCF methods in
656 more diverse phylogenetic and functional sampling of primates.
657
658 **Figure 11 Here**
659 **Figure 12 Here**
660
661 But which of these three methods correlates best with quantified levels of suspensory
662 locomotion (i.e., with real-world behavioral data)? To assess this, we performed non-parametric
663 Spearman correlations of mean PC1 scores, IA values and *a* coefficients (again from the same
664 100 landmark datasets obtained in this study) with mean time spent suspensory as a proportion of
665 total locomotor behavior (reported in Rein, 2011) at the genus level for a subset of our sample
666 (Table 3). Recognizing the small sample size in this comparison, results did show that the
667 proportion of time a genus has been reported to be suspensory was not significantly correlated
668 with the *a* coefficient (r_s=0.618; p=0.153), but was with IA (r_s=0.946; p=0.005) and PC1 scores
669 (r_s=-0.982; p=0.002). Note that the correlation with PC1 scores was slightly higher than the
670 correlation with IA values, again suggesting that the 2DGM analysis does a better job than the
671 IA method in identifying suspensory taxa. The latter finding in particular may further influence
672 functional morphologists and paleoanthropologists to adopt this novel alternative method to

673 quantitatively assess phalangeal curvature in their future research.
674
675 **Table 3 Here**
676
677 **4. Summary and Conclusions**
678 A number of different metrics have been employed to assess and compare phalangeal
679 curvature in living and fossil primates. The most common are the included angle (measured in
680 degrees; Stern, Jungers & Susman, 1995) which assumes that the proximal phalanx represents a
681 portion of an arc of a circle (Fig. 2A), and the *a* coefficient of a second-degree polynomial (via
682 polynomial curve fitting or PCF; Deane, Kremer & Begun, 2005) which assumes that the bone
683 represents the shape of a parabola (Fig. 2B). Although not identical, both methods and metrics
684 generally produce similar results (Fig. 2C) with an acceptable amount of discriminatory power
685 between primate taxa that are highly suspensory (i.e., with more curved proximal phalanges) and
686 taxa that are more terrestrial and quadrupedal (i.e., with flatter proximal phalanges) (Fig. 1; Rein,
687 2011; Deane & Begin, 2008). However, both methods also have a number of drawbacks. One is
688 the high degree of inter-study variability in published included angle values for several
689 commonly studied primates like chimpanzees and macaques (Patel & Maiolino, 2016). Also
690 notable is the fact that as currently implemented, PCF quantifies only the dorsal contour of the
691 proximal phalanx's diaphysis (Deane, Kremer & Begun, 2005) which is less biomechanically
692 meaningful than the curvature of its central longitudinal axis (e.g., Richmond, 2007).
693 Additionally, both approaches often yield some counterintuitive results based on predicted form-
694 function relationships. For instance, calculating included angles from lateral view photographs,
695 often results in no significant differences between gorillas (terrestrial quadrupeds/climbers) and
696 bipedal humans (e.g., Prang et al., 2021). Similarly, brachiating gibbons are not significantly
697 different from arboreal quadrupedal monkeys and African apes (e.g., Böhme et al., 2019) when
698 calculating the *a* coefficient with PCF from lateral view photographs of the diaphysis' dorsal
699 contour. Because phalangeal curvature has been an important variable to assess locomotor and
700 positional behavior in paleoanthropological research (e.g., Stern & Susman, 1983; Jungers et al.,
701 1997; Deane & Begun, 2008; Zhang, Harrison, & Ji, 2020), especially in fossil hominins and
702 fossil non-human apes, it is necessary to consistently and more accurately (i.e., track known
703 behavioral lines) assess curvature across a diverse range of primates.

704 The present study was conducted to develop and test a new alternative method - that is
705 repeatable and biomechanically meaningful using geometric morphometric (GM) techniques - to
706 quantify proximal phalanx diaphysis shape that reflects dorsopalmar curvature. The 2DGM
707 method presented here is not sensitive to inter- and intra-observer error or the digit studied
708 (mPP2 vs. mPP3 vs. mPP4 vs. mPP5). Even the overall quality of the 3D model did not have a
709 major impact on the results (see Supplemental Information) as long as it has a surface mesh of at
710 least 100,000 triangles that does not contain any erroneous spikes, depressions, or holes
711 (including the removal of any naturally occurring nutrient foramina). Accordingly, the source of
712 the 3D surface data (e.g., photogrammetry, laser scan, CT scan, μCT scan) matters little, thus
713 making the method applicable to many more users in the research community (see also Tocheri
714 et al., 2011; Robinson & Terhune, 2017; Shearer at et al., 2017). However, users of this 2DGM
715 method should be mindful to orient the virtual phalanx prior to any subsequent steps using our
716 'gold standard' orientation (as described above; Fig. 3A). The latter is particularly important if
717 users want to use the complete set of landmark data provided in the online Supplemental
718 Information.
719 Overall, the results of our 2DGM analyses demonstrate that differences in diaphysis
720 shape reflective of dorsopalmar curvature across taxa derive from real biological inter- and
721 intraspecific variation. Specifically, assessing curvature shape of the dROI (i.e., the bone's
722 central longitudinal axis excluding proximal and distal articular ends) proves to be useful as PC1
723 scores (which accounted for >80% of total sample variation) distinguish extant taxa along known
724 locomotor behavioral lines. The most suspensory primates such as orangutans, gibbons,
725 siamangs, and spider monkeys still clearly have more curved proximal phalanges compared to
726 stereotypical quadrupedal species (both arboreal and terrestrial) such as proboscis monkeys and
727 baboons, as well as bipedal humans. However, in the new 2DGM approach, different orangutan
728 species can be differentiated, gorilla proximal phalanges are now observed to be significantly
729 more curved than humans, and gibbon proximal phalanges are now observed to be significantly
730 more curved than African apes and monkeys (except suspensory spider monkeys). Therefore, we
731 contend that the 2DGM approach offers even greater discriminating power compared to using IA
732 and PCF especially with regards to degree of forelimb suspension used by living primates.
733 Whether this approach can better differentiate habitually arboreal vs. terrestrial quadrupedal
734 monkeys, however, needs further testing. Additionally, while PC1 scores were significantly

735 correlated with both the included angle and the *a* coefficient of a second-degree polynomial
736 fitted to the same landmark datasets, PC1 scores had a significantly higher correlation with
737 included angles suggesting that a circle model for phalangeal curve shape might be more
738 appropriate than a parabola model. But, we do emphasize that PC scores are not equivalent to IA
739 (measured in degrees) and cannot be used interchangeably.
740 Compared to using IA as is currently implemented (e.g., lateral view photographs,
741 Microscribe point digitizer), some readers of this technical note may consider the 2DGM method
742 presented here too complex and time intensive given that it yields results generally similar to
743 those obtained from other methods. We acknowledge that our approach has more steps and using
744 IA as currently implemented still has some value. For example, limiting comparisons between
745 closely related taxa that are behaviorally different like bipedal humans, quadrupedal
746 chimpanzees and suspensory orangutans (e.g. Stern, Susman & Jungers, 1995; Wallace, Burgess
747 & Patel, 2020) produces results that could be used to generalize the locomotor behaviors of some
748 fossil hominins (e.g., Stratford et al., 2016). But similar comparisons that include more
749 phylogenetic and behavioral diversity of extant and fossil primates often produce results that do
750 not clearly reflect with known or inferred locomotor behaviors (Prang et al., 2021).
751 In summary, we maintain that our 2DGM approach is a worthwhile alternative to assess
752 dorsopalmar curvature because: 1) 2DGM does not assume *a priori* portion of an arc of a circle
753 or parabola model; 2) the developed method has very low intra- and inter-observer variation
754 relative to the variation seen within and among taxa; 3) resulting PC scores show improved
755 extant group separation along known behavioral lines; and 4) resulting PC scores have higher
756 correlation with quantified behavioral data than other metrics. Finally, one other benefit of our
757 landmark-based approach is that the derived 100 landmarks can still be used to quantify IA and *a*
758 coefficient if a researcher still prefers these metrics over PCA on shape coordinates, but with the
759 added benefit that now both IA and *a* metrics will be derived from the more biomechanically
760 relevant central longitudinal axis of the phalanx. To conclude, the outcomes of this technical
761 study demonstrate that proximal phalanx diaphysis shape reflecting longitudinal dorsopalmar
762 curvature determined from 2DGM methods should prove to be useful for addressing additional
763 questions on the functional morphology of primate hands, as well as future paleoanthropological
764 research that involves reconstructing behavior in the fossil record.
765

Acknowledgements

We thank the curators and collections managers at the following museums that facilitated access to specimens in their care: American Museum of Natural History; Academy of Natural Sciences of Drexel University; Natural History Museum of Los Angeles County; Harvard University's Museum of Comparative Zoology; Royal Museum for Central Africa; Smithsonian Institution's National Museum of Natural History; University of the Witwatersrand. Andrew Deane also generously shared *Gorilla b. beringei* data obtained with assistance from the Mountain Gorilla Skeleton Project (MGSP); more details and funding information for the MGSP is available at: www.gwprimatelifehistorylab.org/mountain-gorilla-skeletal-project.

We are also grateful to the staff at the following institutions that assisted us with CT and µCT scanning: University of Southern California's Molecular Imaging Center which receives funding from the National Institutes of Health (NIH S10 RR027665 01); Department of Biomedical Engineering at Stony Brook University; Department of Radiology at Stony Brook University School of Medicine; and the Smithsonian Institution's National Museum of Natural History.

Funding for this research was generously provided by: National Science Foundation (BCS #1317047 to B.A.P.; BCS #1539741 to C.M.O.); the L.S.B. Leakey Foundation (to B.A.P.); the Wenner-Gren Foundation (to C.M.O.); AEI/FEDER EU (CGL2017-82654-P to S.A.), Generalitat de Catalunya (CERCA Programme to S.A.); the University of Southern California's URAP program (to B.A.P.), and the University of Southern California's Office of the Provost (to S.E.W.).

Author contributions

B.A.P. designed the study; B.A.P., C.M.O., S.A. and M.W.T. obtained the raw image and scan data and created the 3D surface models; S.E.W. collected the landmark data; K.L.L. implemented the R script for the 2DGM analyses; S.E.W., K.L.L. and B.A.P. performed the analyses; B.A.P. and S.E.W. drafted the manuscript; all authors reviewed and approved the final version of the manuscript.

Conflict of Interest

The authors declare no conflict of interests.

Data availability statement

R script for performing 2D geometric morphometrics on 100 landmarks of primate proximal phalanges to assess longitudinal curvature shape used in this study is available in the online Supplemental Information. *Morphologika* data files for all specimens (n=378) used in this study is also available in the online Supplemental Information. 3D surface models illustrated in Figure 1 are available on MorphoSource.org as part of project "Anthropoid Primate Hands", the details of which are provided in Appendix Table 1.

References

Adams, D. C., Collyer, M. L., & Kaliontzopoulou, A. (2019). Geomorph: software for geometric morphometric analyses. https://cran.r-project.org/package=geomorph

Birdal, T. (2021). Maximum Inscribed Circle using Distance Transform (https://www.mathworks.com/matlabcentral/fileexchange/30805-maximum-inscribed-circle-using-distance-transform), MATLAB Central File Exchange. Retrieved March 1, 2021.

Böhme, M., Spassov, N., Fuss, J., Tröscher, A., Deane, A. S., Prieto, J., Kirscher, U., Lechner, T., & Begun, D. R. (2019). A new Miocene ape and locomotion in the ancestor of great apes and humans. *Nature*. 575, 1–20. https://doi.org/10.1038/s41586-019-1731-0

Boyer, D. M., Puente, J., Gladman, J. T., Glynn, C., Mukherjee, S., Yapuncich, G. S., & Daubechies, I. (2015). A new fully automated approach for aligning and comparing shapes. *Anatomical Record*. 298, 249–276. https://doi.org/10.1002/ar.23084

Burgess, M. L. (2018). Ontogenetic Changes in Limb Bone Structural Properties and Locomotor Behavior in *Pan.* Ph.D. Dissertation, Johns Hopkins University, Baltimore.

Burri, O., & Guiet, R. (2016). https://imagej.net/Max_Inscribed_Circles.

Byron, C., & Covert, H. (2004). Unexpected locomotor behaviour: brachiation by an Old World monkey (*Pygathrix nemaeus*) from Vietnam. *Journal of Zoology*. 263, 101–106. http://doi.org/10.1017/S0952836904004935

Carlson, K. J. (2005). Investigating the form-function interface in African apes: Relationships between principal moments of area and positional behaviors in femoral and humeral diaphyses. *American Journal of Physical Anthropology*. 127, 312-334. http://doi.org/10.1002/ajpa.20124.

Deane, A. S., & Begun, D. R. (2008). Broken fingers: retesting locomotor hypotheses for fossil hominoids using fragmentary proximal phalanges and high-resolution polynomial curve fitting (HR-PCF). *Journal of Human Evolution*. 55, 691–701. https://doi.org/10.1016/j.jhevol.2008.05.005

Deane, A. S., Kremer, E. P., & Begun, D. R. (2005). New approach to quantifying anatomical curvatures using high-resolution polynomial curve fitting (HR-PCF). *American Journal of Physical Anthropology*. 128, 630–638. https://doi.org/10.1002/ajpa.20202

De Groote, I., Lockwood, C. A., & Aiello, L. C. (2010). Technical note: A new method for measuring long bone curvature using 3D landmarks and semi-landmarks. *American Journal of Physical Anthropology*. 141, 658-664. https://doi.org/10.1002/ajpa.21225

Delgado, R. A., & van Schaik, C. P. (2000). The behavioral ecology and conservation of the orangutan (*Pongo pygmaeus*): a tale of two islands. *Evolutionary Anthropology*. 9, 201–218. https://doi.org/10.1002/1520-6505(2000)9:5%3C201::AID-EVAN2%3E3.0.CO;2-Y

Domínguez-Rodrigo, M., Pickering, T. R., Almécija, S., Heaton, J. L., Baquedano, E., Mabulla, A., & Uribelarrea, D. (2015). Earliest modern human-like hand bone from a new >1.84-million-year-old site at Olduvai in Tanzania. *Nature Communications*. 6, 7987. https://doi.org/10.1038/ncomms8987

Fernández, P. J., Almécija, S., Patel, B. A., Orr, C. M., Tocheri, M. W., & Jungers, W. L. (2015). Functional aspects of metatarsal head shape in humans, apes, and Old World monkeys. *Journal of Human Evolution*. 86, 136–146. https://doi.org/10.1016/j.jhevol.2015.06.005

Granatosky, M. C. (2018). A review of locomotor diversity in mammals with analyses exploring the influence of substrate use, body mass and intermembral index in primates. *Journal of Zoology*. 306, 207–216. https://doi.org/10.1111/jzo.12608

Hammer, Ø., Harper, D. A. T., & Ryan, P. D. (2001). PAST: Paleontological statistics software package for education and data analysis. *Palaeontologia Electronica*. 4, art. 4.

Hamrick, M. W., Meldrum, D. J., & Simons, E. L. (1995). Anthropoid phalanges from the Oligocene of Egypt. *Journal of Human Evolution*. 28, 121–145. https://doi.org/10.1006/jhev.1995.1011

Harmand, W., Lewis, J. E., Feibel, C. S., Lepre, C. J., Prat, S., Lenoble, A., Boës, X., Quinn, R. L., Brenet, M., Arroyo, A., Taylor, N., Clément, S., Daver, G., Brugal, J., Leakey, L., Mortock, R. A., Wright, J. D., Lokorodi, S., Kirwa, C., Kent, D. V., & Roche, H. (2015). 3.3-million-year old stone tools from Lomekwi 3, West Turkana, Kenya. *Nature*. 521, 310-315. https://doi.org/10.1038/nature14464

Jungers, W. L., Godfrey, L. R., Simons, E. L., & Chatrath, P. S. (1997). Phalangeal curvature and positional behavior in extinct sloth lemurs (Primates, Palaeopropithecidae). *Proceedings of the National Academy of Sciences*. 94, 11998–12001. https://doi.org/10.1073/pnas.94.22.11998

Jungers, W. L., Godfrey, L. R., Simons, E. L., Wunderlich, R. E., Richmond, B. G., & Chatrath, P.S. (2002). Ecomorphology and behavior of giant extinct lemurs from Madagascar. In: Plavcan, J.M., Kay, R.F., Jungers, W.L., van Schaik, C.P. (Eds.), *Reconstructing Behavior in the Primate Fossil Record*. Kluwer Academic/Plenum Publishers, New York, pp. 371–411. https://doi.org/10.1007/978-1-4615-1343-8_10

889 Kivell, T. L., Deane, A. S., Tocheri, M. W., Orr, C. M., Schmid, P., Hawks, J., Berger, L. R., &
890 Churchill, S. E. (2015). The hand of *Homo naledi*. *Nature Communications*. 6, 8431.
891 https://doi.org/10.1038/ncomms9431
892
893 Kivell, T. L., Kibii, J. M., Churchill, S. E., Schmid, P., & Berger, L. R. (2011). *Australopithecus*
894 *sediba* hand demonstrates mosaic evolution of locomotor and manipulative abilities. *Science*.
895 333, 1411–1417. https://doi.org/10.1126/science.1202625
896
897 Kivell, T. L., Lemelin, P., Richmond, B. G., & Schmitt, D. (2016). *The Evolution of the Primate*
898 *Hand: Anatomical, Developmental, Functional, and Paleontological Evidence*. Springer, New
899 York. http://doi.org/10.1007/978-1-4939-3646-5
900
901 Matarazzo, S. (2008). Knuckle walking signal in the manual digits of *Pan* and *Gorilla*. *American*
902 *Journal of Physical Anthropology*. 135, 27–33. https://doi.org/10.1002/ajpa.20701
903
904 Matarazzo, S. (2013). Manual pressure distribution patterns of knuckle-walking apes. *American*
905 *Journal of Physical Anthropology*. 152, 44–50. https://doi.org/10.1002/ajpa.22325
906
907 Milne, N., & Granatosky, M. C. (2021). Ulna curvature in arboreal and terrestrial primates.
908 *Journal of Mammalian Evolution*. 28, 897-909. http://doi.org/10/1007/s10914-021-09566-5
909
910 Napier, J. R. (1993). *Hands* [Revised by Russell H. Tuttle]. Princeton University Press,
911 Princeton.
912
913 Neufuss, J., Robbins, M. M., Baeumer, J., Humle, T., & Kivell, T. L. (2017). Comparison of
914 hand use and forelimb posture during vertical climbing in mountain gorillas (*Gorilla beringei*
915 *beringei*) and chimpanzees (*Pan troglodytes*). *American Journal of Physical Anthropology*. 164,
916 651–664. https://doi.org/10.1002/ajpa.23303
917
918 Nguyen, N. H., Pahr, D. H., Gross, T., Skinner, M. M., & Kivell, T. L. (2014). Micro-finite
919 element (μFE) modeling of the siamang (*Symphalangus syndactylus*) third proximal phalanx: the

functional role of curvature and the flexor sheath ridge. *Journal of Human Evolution*. 67, 60–75. https://doi.org/10.1016/j.jhevol.2013.12.008

Patel, B. A. (2010). Functional morphology of cercopithecoid primate metacarpals. *Journal of Human Evolution*. 58, 320–337. https:/doi.org/10.1016/j.jhevol.2010.01.001

Patel, B. A., & Maiolino, S. A. (2016). Morphological diversity in the digital rays of primate hands. In: Kivell, T. L., Lemelin, P., Richmond, B. G., & Schmitt, D. (Eds.), *The Evolution of the Primate Hand: Anatomical, Developmental, Functional, and Paleontological Evidence*. Springer, New York, pp. 55–100. https://doi.org/10.1007/978-1-4939-3646-5_4

Patel, B. A., Yapuncich, G. S., Tran, C., & Nengo, I. O. (2017). Catarrhine hallucal metatarsals from the early Miocene site of Songhor, Kenya. *Journal of Human Evolution*. 108, 176–198. https://doi.org/10.1016/j.jhevol.2017.03.013

Prang, T. C., Ramirez, K., Grabowski, M., & Williams, S. A. (2021). *Ardipithecus* hand provides evidence that humans and chimpanzees evolved from an ancestor with suspensory adaptations. *Sciences Advances*. 7, eabf2474. http://doi.org/10.1126/sciadv.abf2474

Preuschoft, H. (1973a). Body posture and locomotion in some east African Miocene Dryopithecinae. In: Day, M. H. (Ed.), *Human Evolution (Symposium of the Society for the Study of Human Biology, Volume XI)*. Taylor and Francis, London, pp. 13–46.

Preuschoft, H. (1973b). Functional anatomy of the upper extremity. In: Bourne, G. H. (Ed.), *The Chimpanzee, Volume 6*. Karger, Basel, pp. 34–120.

R Core Team. (2019). R: A language and environment for statistical computing. R Foundation for Statistical Computing, Vienna, Austria. https://www.R-project.org/.

Rein, T. R. (2011). The correspondence between proximal phalanx morphology and locomotion: implications for inferring the locomotor behavior of fossil catarrhines. *American Journal of Physical Anthropology*. 146, 435–445. https://doi.org/10.1002/ajpa.21599

Richmond, B. G. (1998). Ontogeny and biomechanics of phalangeal form in primates. Ph.D. Dissertation, State University of New York at Stony Brook, Stony Brook.

Richmond, B. G. (2007). Biomechanics of phalangeal curvature. *Journal of Human Evolution*. 53, 678–690. https://doi.org/10.1016/j.jhevol.2007.05.011

Robinson, C., & Terhune, C. E. (2017). Error in geometric morphometric data collection: Combining data from multiple sources. *American Journal of Physical Anthropology*. 164, 62-75. https://doi.org/10.1002/ajpa.23257

Schneider, C. A., Rasband, W. S., & Eliceiri, K. W. (2012). NIH Image to ImageJ: 25 years of image analysis. *Nature Methods*. 9, 671–675. https://doi.org/10.1038/nmeth.2089

Shearer, B. M., Cooke, S. B., Halenar, L. B., Reber, S. L., Plummer, J. E., Delson, E., & Tallman, M. (2017). Evaluating causes of error in landmark-based data collection using scanners. *PLOS ONE* 12, e0187452. https://doi.org/10.1371/journal.pone.0187452

Spencer, M. A., & Spencer, G. S. (1995). Technical note: video-based three-dimensional morphometrics. *American Journal of Physical Anthropology* 96, 443–453. https://doi.org/10.1002/ajpa.1330960409

Stern, J. T., Jungers, W. L., & Susman, R. L. (1995). Quantifying phalangeal curvature: an empirical comparison of alternative methods. *American Journal of Physical Anthropology*. 97, 1–10. https://doi.org/10.1002/ajpa.1330970102

Stern, J. T., & Susman, R.L. (1983). The locomotor anatomy of *Australopithecus afarensis*. *American Journal of Physical Anthropology*. 60, 279–317. https://doi.org/10.1002/ajpa.1330600302

Stratford, D., Heaton, J. L., Pickering, T. R., Caruana, M. V., & Shadrach, K. (2016). First hominin fossils from Milner Hall, Sterkfontein, South Africa. *Journal of Human Evolution*. 91, 167–173. https://doi.org/10.1016/j.jhevol.2015.12.005

Squyres, N., & DeLeon, V. B. (2015). Clavicular curvature and locomotion in anthropoid primates: A 3D geometric morphometric analysis. *American Journal of Physical Anthropology*. 158, 257-268. https://doi.org/10.1002/ajpa.22785

Susman, R. L., de Ruiter, D., & Brain, C. K. (2001). Recently identified postcranial remains of *Paranthropus* and early Homo from Swartkrans Cave, South Africa. *Journal of Human Evolution*. 41, 607–629. https://doi.org/10.1006/jhev.2001.0510

Susman, R. L., Stern, J. T., & Jungers, W. L. (1984). Arboreality and bipedality in the Hadar hominids. *Folia Primatologica*. 43, 113–156. https://doi.org/10.1159/000156176

Thompson, N. E., Ostrofsky, K. R., McFarlin, S. C., Robbins, M. M., Stoinski, T. S., & Almécija, S. (2018). Unexpected terrestrial hand posture diversity in wild mountain gorillas. *American Journal Physical Anthropology*. 166, 84-94. https://doi.org/10.1002/ajpa.23404

Tocheri, M. W., Orr, C. M., Jacofsky, M. C., & Marzke, M. W. (2008). The evolutionary history of the hominin hand since the last common ancestor of *Pan* and *Homo*. *Journal of Anatomy*. 212, 544-562. https://doi.org/10.1111/j.1469-7580.2008.00865.x

Tocheri, M. W., Solhan, C. R., Orr, C. M., Femiani, J., Frohlich, B., Groves, C. P., Harcourt-Smith, W. E., Richmond, B. G., Shoelson, B., & Jungers, W. L. (2011). Ecological divergence and medial cuneiform morphology in gorillas. *Journal of Human Evolution*. 60, 171-184. https://doi:10.1016/j.jhevol.2010.09.002

Tuttle, R. H. (1970). Postural, propulsive, and prehensile capabilities in the cheiridia of chimpanzees and other great apes. In: Bourne, G. H. (Ed.), *The Chimpanzee, Volume 2*. Karger, Basel, pp. 167–253.

Wallace, I. J., Burgess, M. L., & Patel, B. A. (2020). Phalangeal curvature in a chimpanzee raised like a human: Implications for inferring arboreality in fossil hominins. *Proceedings of the National Academy of Sciences*. 117, 11223–11225. https://doi.org/10.1073/pnas.2004371117

Zhang, Y. Q., Harrison, T., & Ji, X. P. (2020). Inferring the locomotor behavior of fossil hominoids from phalangeal curvature using a novel method: *Lufengpithecus* as a case study. *Acta Anthropologica Sinica*. 39, 532-554. https://doi.org/10.16359/j.cnki.cn11-1963/q.2020.0061

Figure Legends

Figure 1. Primate proximal phalanges. Representative 3D surface models (top; silver color) and mid-sagittal planes (bottom; black color) of manual proximal phalanges of digit 3 (mPP3) in medial views. The proximal ends of the phalanges are to the left and the distal ends are to the right. All bones are from the right side or have been mirror-imaged to depict right side elements (as noted in Table S1). One hundred landmarks (yellow filled spheres) within the mid-sagittal plane show the central proximodistal axis and illustrates diaphysis shape reflecting its dorsopalmar curvature. Abbreviations: POA, *Pongo abelii* (USNM-143598; female); POP, *Pongo pygmaeus* (USNM-145306; female; mirror-imaged); SS, *Symphalangus syndactylus* (USNM-143579; female); HY, *Hylobates agilis* (AMNH-103667, male); PT, *Pan troglodytes* (USNM-176228; male); PP, *Pan paniscus* (RMCA-20881; male; mirror-imaged); GG, *Gorilla gorilla* (AMNH-54355; male); GBB, *Gorilla beringei beringei* (USNM-545041; male; mirror-imaged); HS, *Homo sapiens* (USNM-437R; female); AT, *Ateles paniscus* (USNM-361027; male; mirror-imaged); PAP, *Papio cynocephalus* (USNM-452509; male); NL, *Nasalis larvatus* (AMNH-106275; male). All individuals have been scaled to the same interarticular length of the mid-sagittal plane. Scale bars for each individual are below its surface model and equal 1 cm. The 3D surface models of each specimen illustrated are available for further study on www.MorphoSource.org (see Appendix Table 1 for more details).

Figure 2. Current methods to measure phalanx curvature. A) Included angles - an arc of a circle model of curvature - shown for a highly curved proximal phalanx of *Pongo abelii* (top; Θ^1; red dashed line half-circle) and a straight proximal phalanx of *Homo sapiens* (bottom; Θ^2; red solid line half-circle); note that $\Theta^1 > \Theta^2$. B) Second-degree polynomials – a parabola model of curvature - shown for a highly curved proximal phalanx of *Pongo abelii* (top; a^1; blue dashed line parabola) and a straight proximal phalanx of *Homo sapiens* (bottom; a^2; blue solid line parabola); note that $a^1 > a^2$. C) Bivariate scatter plot of mean included angles (from Rein, 2011) vs. median polynomial curve fitting *a* coefficients (from Dean & Begun, 2008) in a sample of extant apes and monkeys showing close, but less than ideal, correlation.

Figure 3: 2D landmark acquisition. A) 3D surface model of a manual proximal phalanx of

digit 3 in *Pongo abelii* (USNM-143598) shown in the standardized anatomical orientation (i.e., the 'gold' standard orientation) as defined in the text. B) Illustration depicting a hollow surface mesh being voxelized (i.e., virtually filled) and resliced yielding 1000 evenly spaced binary slices along the length of the entire bone. C) The 1000 binary slices are cropped to create a new region of interest of the diaphysis (dROI; pink shaded region) as defined in the text, from which a new hollow surface mesh is created of the dROI, and subsequently the dROI is again voxelized and resliced yielding 100 evenly spaced binary slices. D) The centroid of each of the 100 binary slices of the dROI is determined using the Max Inscribed Circle plugin for ImageJ software as defined in the text. The y- and z-coordinates of the centroids ultimately serve as the landmarks for the 2DGM analyses to quantify diaphysis shape.

Figure 4: Error analysis – specimen orientation. Procrustes distances between the gold standard specimen and 60 variants of different orientation plotted against change in degrees in reference to the gold standard specimen. The insert shows a manual proximal phalanx of digit 3 in *Pongo abelii* (USNM-143598) rotated about its central axis of rotation between 1-10 degrees from its 'gold standard' orientation (as defined in the text and shown in Figure 3A) in the dorsal, palmar, medial, lateral, clockwise, counterclockwise directions. Among the 60 variants, Procrustes distances differed inconsequentially when the specimen moved from the gold standard in medial, lateral, clockwise, and counterclockwise directions, but Procrustes distances increased linearly when the oriented bone was incorrectly positioned in the dorsal and palmar directions.

Figure 5: Error analysis – dROI determination. Box-and-whiskers plots of Procrustes distances of intra- and inter-observer error evaluating specimen dROI determination. Blue and red boxes show intra-observer Procrustes distances (n=45 comparisons for each) and the purple box shows inter-observer Procrustes distances (n=100 comparisons) for the tested *Pongo abelii* specimen (*Pongo abelii* USNM-143598). The gray box shows Procrustes distances between all *Pongo abelii* specimens (n=136 comparisons). Horizontal lines within each box illustrate the median of the distribution. Boxes envelop the inter quartile range (50% of values) of the sample distribution, and whiskers encompass the range excluding outliers. Filled circles beyond whiskers indicate outliers. Overall species variation (gray box) indicates that any minor

differences in cropping (as defined in the text and shown in Figure 3) within and between observers of a single specimen is negligible in larger scale comparisons within and among taxa.

Figure 6. **Error analysis – complete protocol**. Box-and-whiskers plots of Procrustes distances of intra- and inter-observer error evaluating the complete protocol. Blue and red boxes show intra-observer Procrustes distances (n=45 comparisons for each) and the purple box shows inter-observer Procrustes distances (n=100 comparisons) for the tested *Pongo abelii* specimen (*Pongo abelii* USNM-143598). The gray box shows Procrustes distances between all *Pongo abelii* specimens (n=136 comparisons). Horizontal lines within each box illustrate the median of the distribution. Boxes envelop the inter quartile range (50% of values) of the sample distribution, and whiskers encompass the range excluding outliers. Filled circles beyond whiskers indicate outliers. Overall species variation (gray box) indicates that any minor differences in implementing the complete protocol (as defined in the text and shown in Figure 3) within and between observers of a single specimen is trivial in larger scale comparisons within and among taxa.

Figure 7. Inter-digit variation. Box-and-whiskers plots of PC1 scores for the analysis evaluating curvature shape across manual proximal phalanges of digits 2-5 (PP2-PP5) in *Pongo abelli* (left, filled boxes) and *Homo sapiens* (right, open boxes), two species with curved and flat phalanges, respectively. Horizontal lines within each box illustrate the median of the distribution. Boxes envelop the inter quartile range (50% of values) of the sample distribution, and whiskers encompass the range excluding outliers. Filled circles beyond whiskers indicate outliers. Despite some variation across digits there were no significant differences (p>0.05) in any of the comparisons in either species.

Figure 8: Evaluating 2DGM variation. Bivariate scatter plot of PC1 vs. PC2 scores for the 2DGM analysis evaluating diaphysis shape of manual proximal phalanges in the comparative sample. PC1 accounted for 85.3% of the total variation and represents the overall curvature shape of the bone's diaphysis. Specimens that are more curved are negative on the PC1 axis and those that are flatter are positive (see also Figure 10). The maximum and minimum shapes for PC1 are shown on the left and right sides, respectively (black filled circles are the max and min

shapes; gray filled circles are mean shapes). The maximum and minimum shapes for PC2 are shown in Figure S3. Abbreviations: HS, *Homo sapiens*; PT, *Pan troglodytes*; PP, *Pan paniscus*; GG, *Gorilla gorilla*; GBB, *Gorilla beringei beringei*; GBG; *Gorilla beringei graueri*; POA, *Pongo abelii*; POP, *Pongo pygmaeus*; SS, *Symphalangus syndactylus*; HY, *Hylobates* spp.; PAP, *Papio* spp.; NL, *Nasalis larvatus*; AT, *Ateles* spp. See Table 1 for additional information about the comparative sample.

Figure 9: Evaluating 2DGM utility. Box-and-whiskers plots of PC1 scores (top panel) and PC2 scores (bottom panel) for the 2DGM analysis evaluating diaphysis shape of manual proximal phalanges in the comparative sample. Specimens that are more curved have smaller (and negative) PC1 scores and those that are flatter have higher (and positive) PC1 scores. Horizontal lines within each box illustrate the median of the distribution. Boxes envelop the inter quartile range (50% of values) of the sample distribution, and whiskers encompass the range excluding outliers. Filled circles beyond whiskers indicate outliers. Specimens ordered from left to right based on mean PC1 score. Abbreviations: HS, *Homo sapiens*; PT, *Pan troglodytes*; PP, *Pan paniscus*; GG, *Gorilla gorilla*; GBB, *Gorilla beringei beringei*; GBG; *Gorilla beringei graueri*; POA, *Pongo abelii*; POP, *Pongo pygmaeus*; SS, *Symphalangus syndactylus*; HY, *Hylobates* spp.; PAP, *Papio* spp.; NL, *Nasalis larvatus*; AT, *Ateles* spp. See Table 1 for additional information about the comparative sample.

Figure 10. **Species mean shapes**. Plots of species mean shapes relative to the sample mean for the 2DGM analysis evaluating manual proximal phalanx diaphysis shape. Black filled circles are species mean Procrustes coordinates; gray filled circles represent the sample mean Procrustes coordinates. The proximal ends of the phalanges are to the left and distal ends are to the right. The dorsal sides of the phalanges are to the top and the palmar sides are to the bottom. Abbreviations: HS, *Homo sapiens*; PT, *Pan troglodytes*; PP, *Pan paniscus*; GG, *Gorilla gorilla*; GBB, *Gorilla beringei beringei*; GBG; *Gorilla beringei graueri*; POA, *Pongo abelii*; POP, *Pongo pygmaeus*; SS, *Symphalangus syndactylus*; HY, *Hylobates* spp.; PAP, *Papio* spp.; NL, *Nasalis larvatus*; AT, *Ateles* spp. See Table 1 for additional information about the comparative sample.

Figure 11. 2DGM vs. included angle. Bivariate scatter plot of PC1 scores vs. included angles (in degrees) evaluating the correlation between different methods of assesses proximal phalangeal curvature in a sample of humans, non-human apes, and monkeys. The correlation is significant (r=-0.940) and higher than the correlation observed between PC1 scores and PCF *a* coefficients (see Figure 12). Abbreviations: HS, *Homo sapiens*; PT, *Pan troglodytes*; PP, *Pan paniscus*; GG, *Gorilla gorilla*; GBB, *Gorilla beringei beringei*; GBG; *Gorilla beringei graueri*; POA, *Pongo abelii*; POP, *Pongo pygmaeus*; SS, *Symphalangus syndactylus*; HY, *Hylobates* spp.; PAP, *Papio* spp.; NL, *Nasalis larvatus*; AT, *Ateles* spp. See Table 1 for additional information about the comparative sample.

Figure 12. 2DGM vs. PCF. Bivariate scatter plot of PC1 scores vs. PCF *a* coefficients evaluating the correlation between different methods of assessing proximal phalangeal curvature in a sample of humans, non-human apes, and monkeys. The correlation is significant (r=-0.753) but is lower than the correlation observed between PC1 scores and included angles (see Figure 11). Abbreviations: HS, *Homo sapiens*; PT, *Pan troglodytes*; PP, *Pan paniscus*; GG, *Gorilla gorilla*; GBB, *Gorilla beringei beringei*; GBG; *Gorilla beringei graueri*; POA, *Pongo abelii*; POP, *Pongo pygmaeus*; SS, *Symphalangus syndactylus*; HY, *Hylobates* spp.; PAP, *Papio* spp.; NL, *Nasalis larvatus*; AT, *Ateles* spp. See Table 1 for additional information about the comparative sample.

Table 1: Comparative sample. [€]

Taxon Code	Taxon	Common Name	Sample size n (f, m, u, sa)	Collection	Acquisition Modality
HS	*Homo sapiens*	Human	70 (20, 23, 27, 0)	SBU, USNM, USC, WITZ	µCT, CT, laser scan
PT	*Pan troglodytes*[$]	Chimpanzee	57 (19, 31, 7, 3)	AMNH, LACM, RMCA, USNM	µCT, CT, laser scan
PP	*Pan paniscus*	Bonobo	21 (12, 9, 0, 0)	AMNH, RMCA	µCT, laser scan
GG	*Gorilla gorilla*	Western Gorilla	27 (8, 17, 2, 1)	AMNH, MCZ, RMCA, USNM	µCT, CT, laser scan
GBB	*Gorilla beringei beringei*	Mountain Gorilla	43 (19, 23, 1, 1)	AMNH, MGSP, RMCA, USNM	µCT, CT, laser scan
GBG	*Gorilla beringei graueri*	Eastern Lowland Gorilla	18 (6, 12, 0, 0)	AMNH, RMCA	µCT, laser scan
POA	*Pongo abelii*	Sumatran Orangutan	17 (9, 8, 0, 7)	USNM	µCT, CT
POP	*Pongo pygmaeus*	Bornean Orangutan	20 (12, 7, 1, 1)	AMNH, USNM	µCT, CT
SS	*Symphalangus syndactylus*	Siamang	9 (5, 2, 2, 2)	AMNH, USNM	µCT
HY	*Hylobates* spp.[#]	Gibbon	33 (12, 18, 3, 4)	AMNH, MCZ, USNM	µCT
NL	*Nasalis larvatus*	Proboscis Monkey	23 (7, 11, 5, 0)	AMNH, ANSP, MCZ	µCT
PAP	*Papio* spp.[†]	Baboon	19 (9, 5, 5, 0)	AMNH, LACM, SBU, USNM	µCT
AT	*Ateles* spp.[§]	Spider Monkey	21 (12, 8, 1, 2)	AMNH, USNM	µCT

[€] Abbreviations: n = total sample size; f = females; m = males; u = unknown sex; sa = subadults; AMNH = American Museum of Natural History; ANSP = Academy of Natural Sciences of Drexel University; MGSP = Mountain Gorilla Skeletal Project; LACM, Natural History Museum of Los Angeles County; MCZ = Harvard University's Museum of Comparative Zoology; RMCA = Royal Museum for Central Africa; SBU = Stony Brook University; USC = University of Southern California; USNM = Smithsonian Institution's National Museum of Natural History; WITS, University of the Witwatersrand.

[$] Includes the following subspecies: *Pan troglodytes schweinfurthii*; *P. t. troglodytes*; *P. t. verus*; and specimens without subspecies information.

[#] Includes the following species: *Hylobates agilis*; *H. klossii*; *H. lar*; *H. moloch*; *H. muelleri*; *Hoolock hoolock*; *Nomascus concolor*; *N. leucogenys*; *N. gabriellae*.

[†] Includes the following species: *Papio anubis*; *P. cynocephalus*; *P. hamadryas*; *P. ursinus*.

[§] Includes the following species: *Ateles belzebuth*; *A. fusciceps*; *A. geoffroyi*; *A. marginatus*; *A. paniscus*.

Table 2: Interspecific variation in proximal phalangeal curvature shape. Results of ANOVA and Tukey's Pairwise Comparisons for PC1 scores (top) and PC2 scores (bottom). Above the diagonal are *p* values; below the diagonal are Tukey's Q values. Taxon codes as in Table 1.

PC1 Scores - ANOVA Results: F=123.00; df=12,365; $p<0.0001$													
	HS	PT	PP	GG	GBB	GBG	POA	POP	SS	HY	NL	PAP	AT
HS	---	0.0065	0.0000	0.0000	0.0041	0.0241	0.0000	0.0000	0.0000	0.0000	0.9996	0.0420	0.0000
PT	5.5090	---	0.9501	0.3655	1.0000	1.0000	0.0000	0.0000	0.0000	0.0000	0.0001	0.0000	0.0000
PP	7.6700	2.1610	---	0.9989	0.9732	0.8032	0.0000	0.0000	0.0000	0.0000	0.0000	0.0000	0.0000
GG	9.0630	3.5540	1.3930	---	0.4476	0.1700	0.0000	0.0000	0.0000	0.0000	0.0000	0.0000	0.0000
GBB	5.6770	0.1676	1.9930	3.3870	---	1.0000	0.0000	0.0000	0.0000	0.0000	0.0001	0.0000	0.0000
GBG	5.0010	0.5083	2.6690	4.0620	0.6758	---	0.0000	0.0000	0.0000	0.0000	0.0007	0.0000	0.0000
POA	31.7100	26.2000	24.0400	22.6400	26.0300	26.7100	---	0.0003	0.0000	0.0000	0.0000	0.0000	0.0000
POP	25.1300	19.6200	17.4600	16.0600	19.4500	20.1200	6.5810	---	0.1103	0.0001	0.0000	0.0000	0.0000
SS	20.8200	15.3200	13.1500	11.7600	15.1500	15.8200	10.8800	4.3000	---	0.7650	0.0000	0.0000	0.6539
HY	18.0700	12.5600	10.4000	9.0030	12.3900	13.0700	13.6400	7.0590	2.7590	---	0.0000	0.0000	1.0000
NL	1.2630	6.7730	8.9330	10.3300	6.9400	6.2640	32.9700	26.3900	22.0900	19.3300	---	0.3915	0.0000
PAP	4.7630	10.2700	12.4300	13.8300	10.4400	9.7640	36.4700	29.8900	25.5900	22.8300	3.5000	---	0.0000
AT	17.8300	12.3300	10.1600	8.7720	12.1600	12.8300	13.8700	7.2910	2.9900	0.2315	19.1000	22.6000	---

PC2 Scores - ANOVA Results: F=61.13; df=12,365; $p<0.0001$													
	HS	PT	PP	GG	GBB	GBG	POA	POP	SS	HY	NL	PAP	AT
HS	---	0.8968	1.0000	0.0000	0.0000	0.0000	0.9909	1.0000	0.8731	0.0014	0.0160	0.0073	0.6320
PT	2.3980	---	0.8850	0.0000	0.0000	0.0000	1.0000	0.9620	0.0325	0.0000	0.0000	0.0000	0.0080
PP	0.0406	2.4390	---	0.0000	0.0000	0.0000	0.9889	1.0000	0.8857	0.0016	0.0177	0.0081	0.6528
GG	12.0900	9.6890	12.1300	---	0.9999	0.9836	0.0000	0.0000	0.0000	0.0000	0.0000	0.0000	0.0000
GBB	13.1500	10.7600	13.1900	1.0660	---	1.0000	0.0000	0.0000	0.0000	0.0000	0.0000	0.0000	0.0000
GBG	13.9600	11.5700	14.0000	1.8760	0.8102	---	0.0000	0.0000	0.0000	0.0000	0.0000	0.0000	0.0000
POA	1.7520	0.6461	1.7930	10.3400	11.4000	12.2100	---	0.9986	0.1260	0.0000	0.0001	0.0000	0.0400
POP	0.3141	2.0840	0.3547	11.7700	12.8400	13.6500	1.4380	---	0.7503	0.0005	0.0070	0.0030	0.4678
SS	2.4770	4.8760	2.4370	14.5700	15.6300	16.4400	4.2300	2.7910	---	0.3640	0.7948	0.6541	1.0000
HY	6.0350	8.4330	5.9940	18.1200	19.1900	20.0000	7.7870	6.3490	3.5570	---	1.0000	1.0000	0.6480
NL	5.1670	7.5650	5.1260	17.2500	18.3200	19.1300	6.9190	5.4810	2.6890	0.8678	---	1.0000	0.9545
PAP	5.4670	7.8650	5.4270	17.5500	18.6200	19.4300	7.2190	5.7810	2.9900	0.5674	0.3004	---	0.8864
AT	3.0330	5.4310	2.9920	15.1200	16.1900	17.0000	4.7850	3.3470	0.5556	3.0020	2.1340	2.4340	---

Table 3: Mean PC1 score, included angle (IA), PCF *a* coefficient, and proportion of time suspensory (SUS). Taxon codes as in Table 1.

Taxon Code	PC1 score	IA (degrees)	*a* coefficient	SUS[#]
HS	0.02214	22.26	0.00600	0.00
PT	0.00743	30.07	0.00597	0.01
GG	-0.00206	33.30	0.00691	0.01
POP	-0.04455	50.12	0.00878	0.59
HY	-0.02610	40.88	0.01151	0.51
PAP	0.03486	17.20	0.00720	0.00
AT	-0.02548	41.09	0.01243	0.28

[#] See citations reported in Rein (2011).

Appendix Table 1. MorphoSource ID numbers for specimens illustrated in Figure 1 of the main text.

Species	Side[#]	Museum ID[$]	MorphoSource Media
Homo sapiens	R	USNM-437R	ark:/87602/m4/M154307
Pan troglodytes	R	USNM-176228	ark:/87602/m4/M154311
Pan paniscus	L→R	RMCA-20881	ark:/87602/m4/M154310
Gorilla b. beringei	L→R	USNM-545041	ark:/87602/m4/M154305
Gorilla gorilla	R	AMNH-54355	ark:/87602/m4/M154306
Pongo abelii	R	USNM-143598	ark:/87602/m4/M154313
Pongo pygmaeus	L→R	USNM-145306	ark:/87602/m4/M154314
Symphalangus syndactylus	R	USNM-143579	ark:/87602/m4/M154315
Hylobates agilis	R	AMNH-103667	ark:/87602/m4/M154308
Papio cynocephalus	R	USNM-452509	ark:/87602/m4/M154312
Nasalis larvatus	R	AMNH-106275	ark:/87602/m4/M154309
Ateles paniscus	L→R	USNM-361027	ark:/87602/m4/M154304

[#] Original side studied (→R = specimen mirror imaged from left to right for analysis).

[$] Museum Abbreviations: AMNH = American Museum of Natural History – Department of Mammalogy; USNM = Smithsonian Institution's National Museum of Natural History – Division of Mammals or Anthropology; RMCA = Royal Museum of Central Africa – Department of Mammalogy.

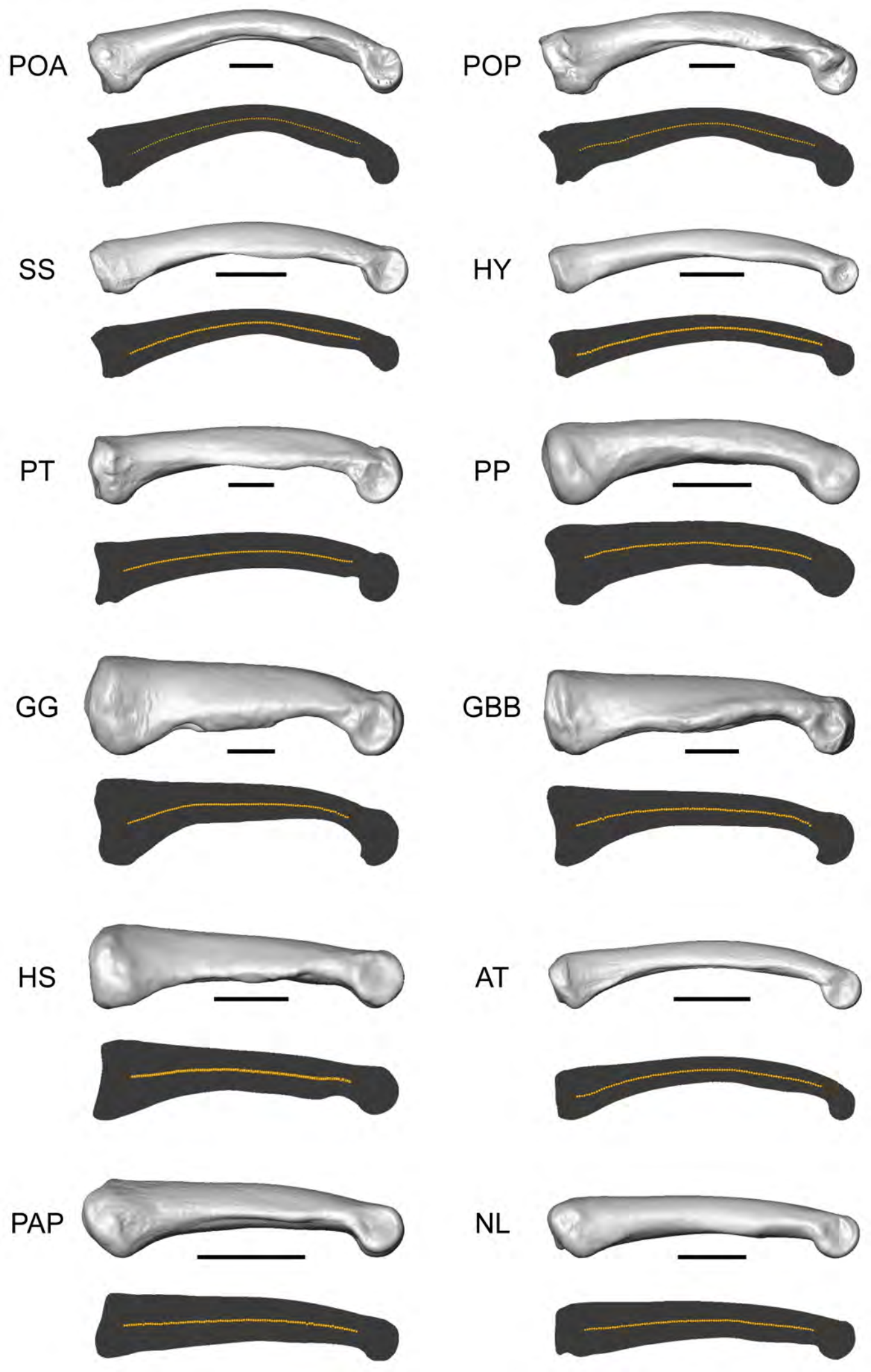
POA
POP
SS
HY
PT
PP
GG
GBB
HS
AT
PAP
NL

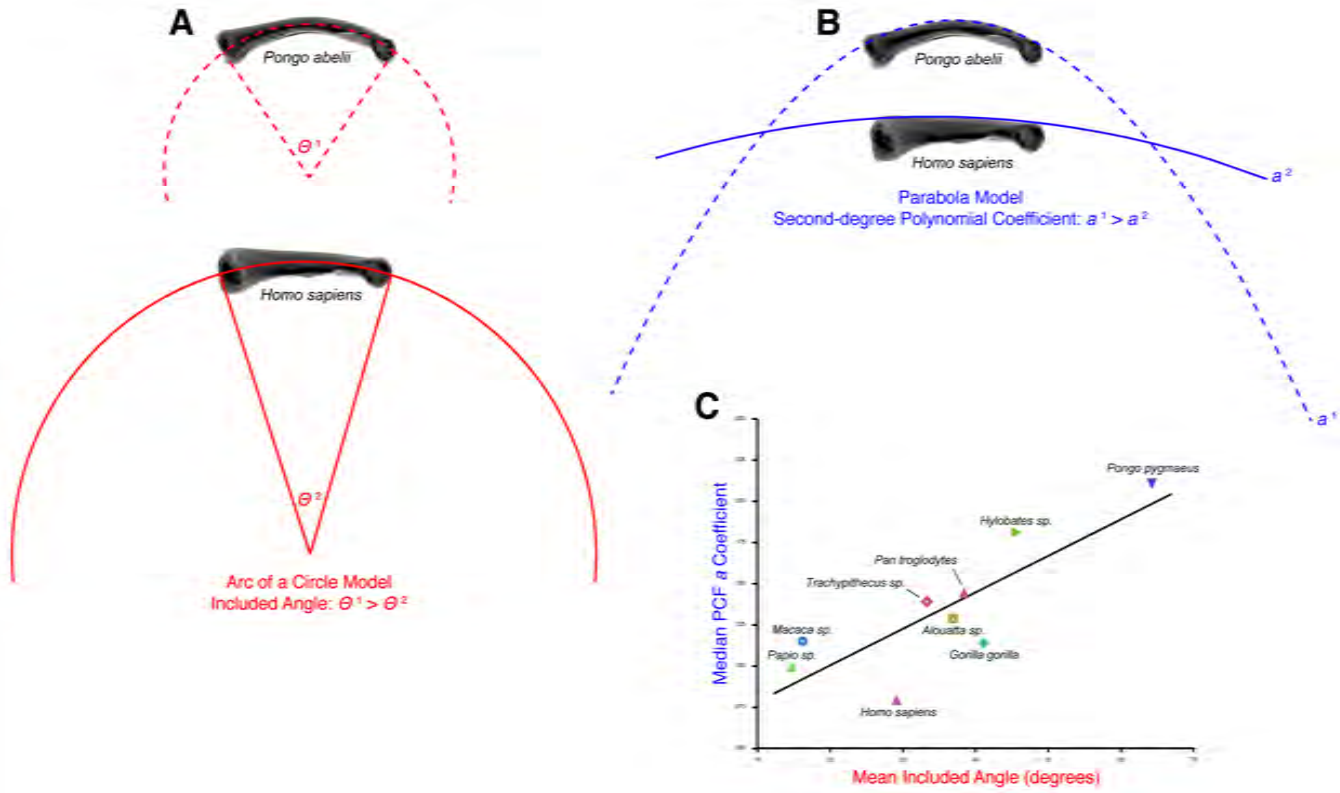
A
Pongo abelii
Θ 1
Homo sapiens
Θ 2
Arc of a Circle Model
Included Angle: Θ 1 > Θ 2
B
Pongo abelii
Homo sapiens
a 2
a 1
Parabola Model
Second-degree Polynomial Coefficient: a 1 > a 2
C
Median PCF a Coefficient
Mean Included Angle (degrees)
Pongo pygmaeus
Hylobates sp.
Pan troglodytes
Trachypithecus sp.
Alouatta sp.
Macaca sp.
Papio sp.
Gorilla gorilla
Homo sapiens

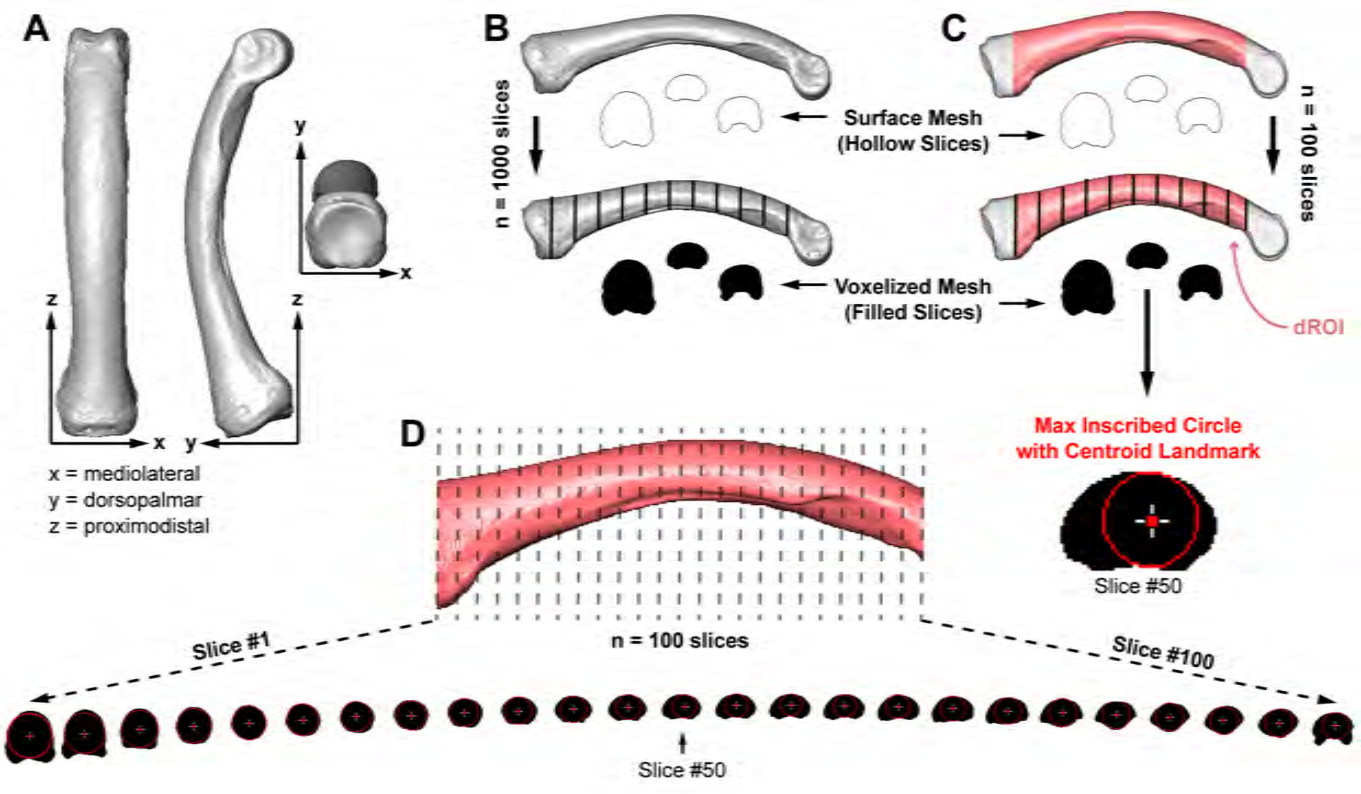
A
y
x
z
z
x
y
x = mediolateral
y = dorsopalmar
z = proximodistal
B
n = 1000 slices
Surface Mesh
(Hollow Slices)
Voxelized Mesh
(Filled Slices)
C
n = 100 slices
dROI
Max Inscribed Circle
with Centroid Landmark
Slice #50
D
n = 100 slices
Slice #1
Slice #100
Slice #50

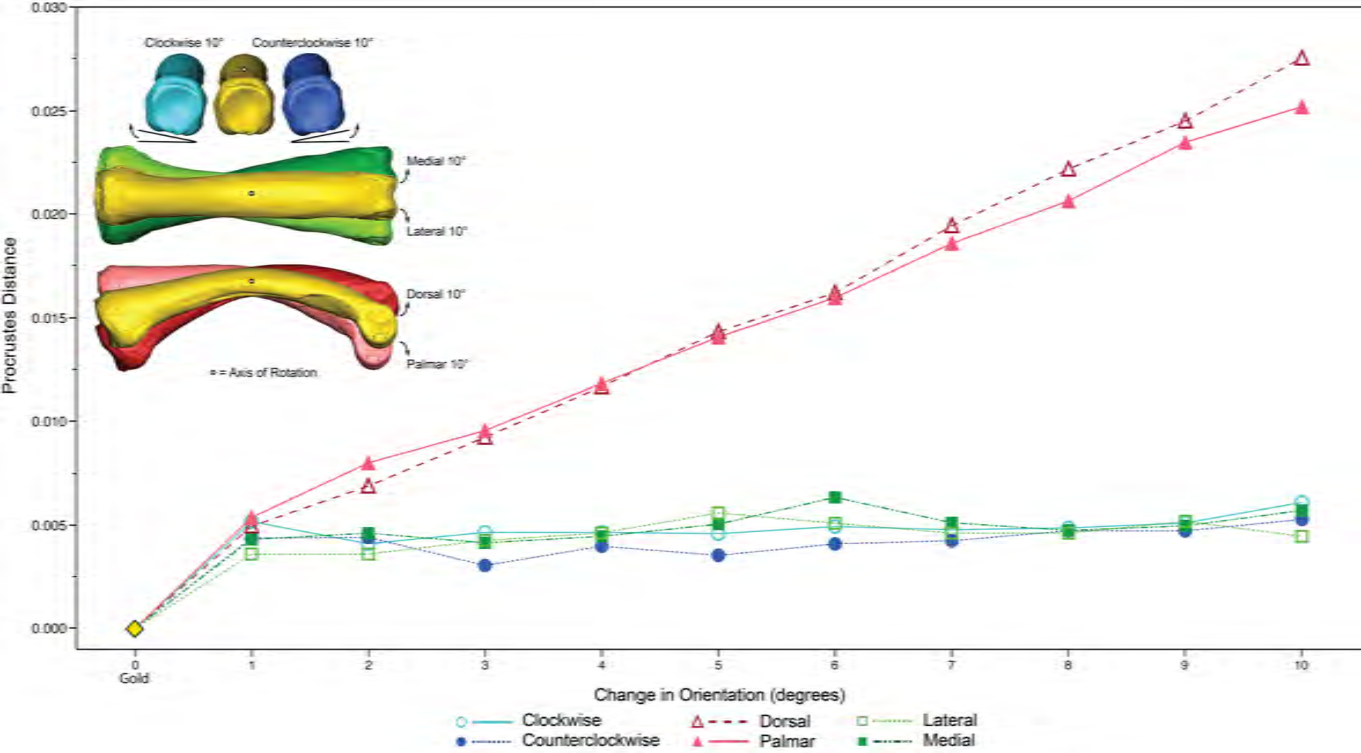
Clockwise 10°
Counterclockwise 10°
Medial 10°
Lateral 10°
Dorsal 10°
Palmar 10°
= Axis of Rotation
Procrustes Distance
0.030
0.025
0.020
0.015
0.010
0.005
0.000
0
Gold
1
2
3
4
5
6
7
8
9
10
Change in Orientation (degrees)
Clockwise
Counterclockwise
Dorsal
Palmar
Lateral
Medial

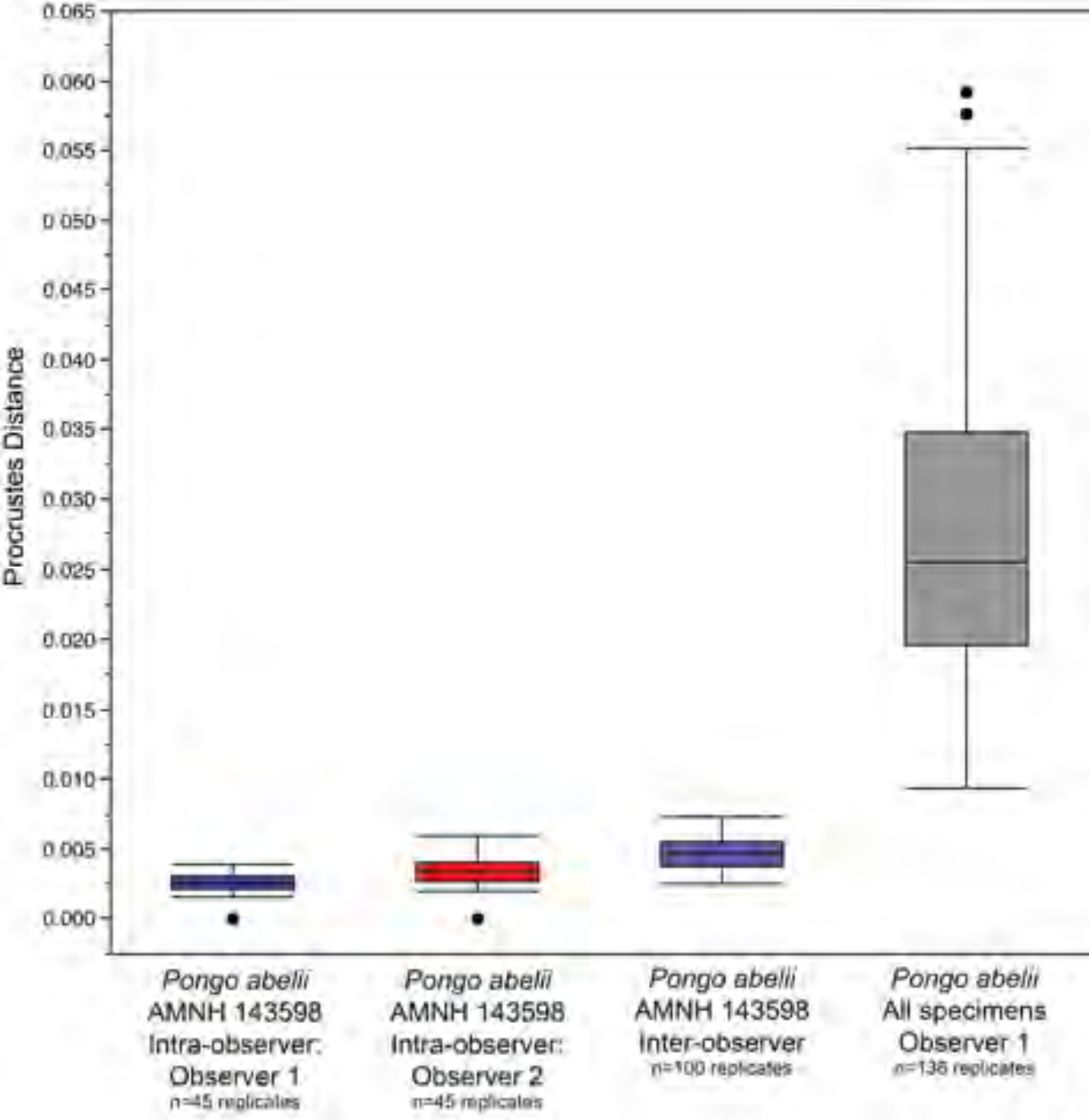
Procrustes Distance
0.065
0.060
0.055
0.050
0.045
0.040
0.035
0.030
0.025
0.020
0.015
0.010
0.005
0.000
Pongo abelii
AMNH 143598
Intra-observer:
Observer 1
n=45 replicates
Pongo abelii
AMNH 143598
Intra-observer:
Observer 2
n=45 replicates
Pongo abelii
AMNH 143598
Inter-observer
n=100 replicates
Pongo abelii
All specimens
Observer 1
n=136 replicates

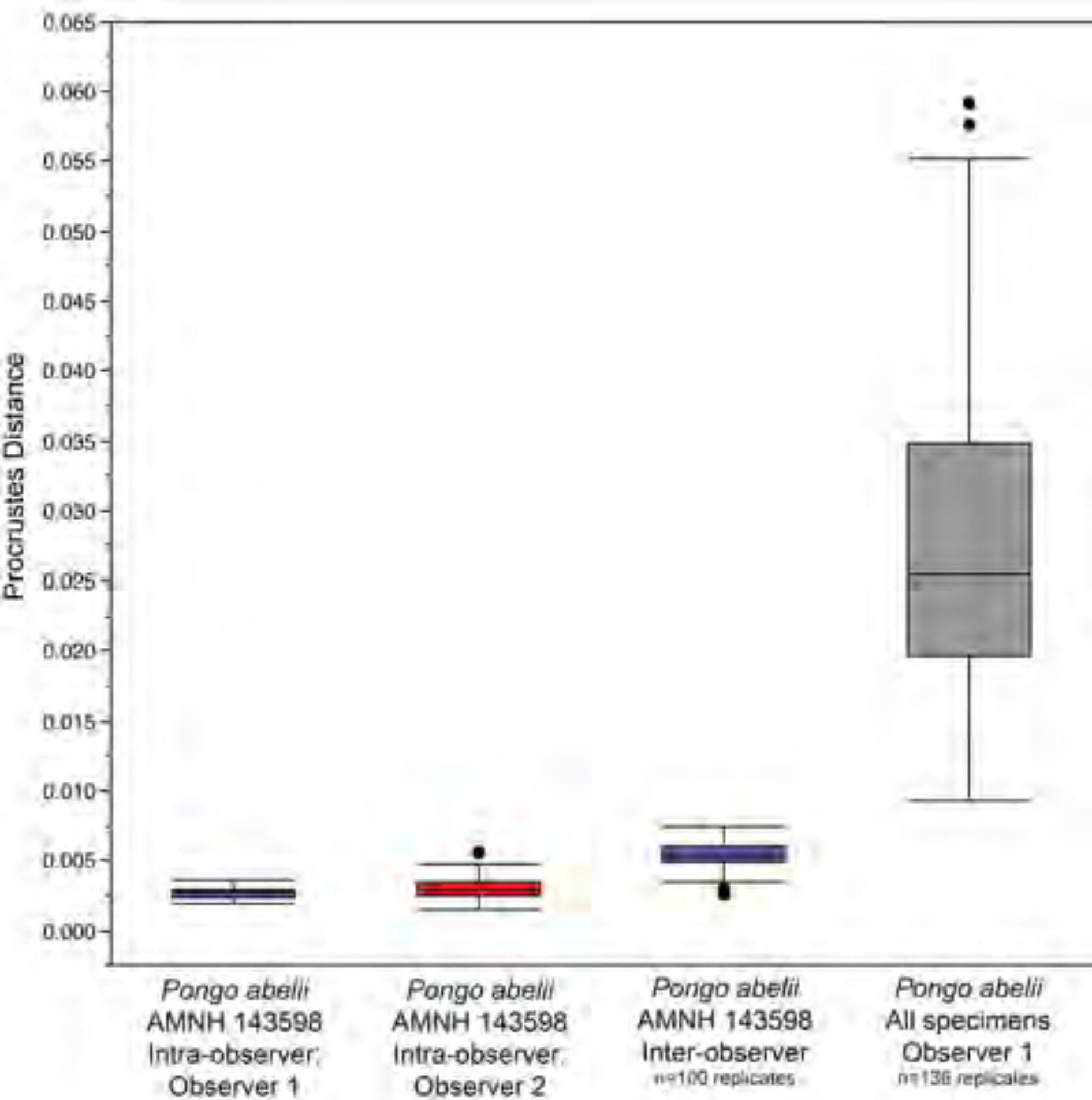
0.065
0.060
0.055
0.050
0.045
0.040
0.035
0.030
0.025
0.020
0.015
0.010
0.005
0.000
Procrustes Distance
Pongo abelii
AMNH 143598
Intra-observer;
Observer 1
n=45 replicates
Pongo abelii
AMNH 143598
Intra-observer;
Observer 2
n=45 replicates
Pongo abelii
AMNH 143598
Inter-observer
n=100 replicates
Pongo abelii
All specimens
Observer 1
n=136 replicates

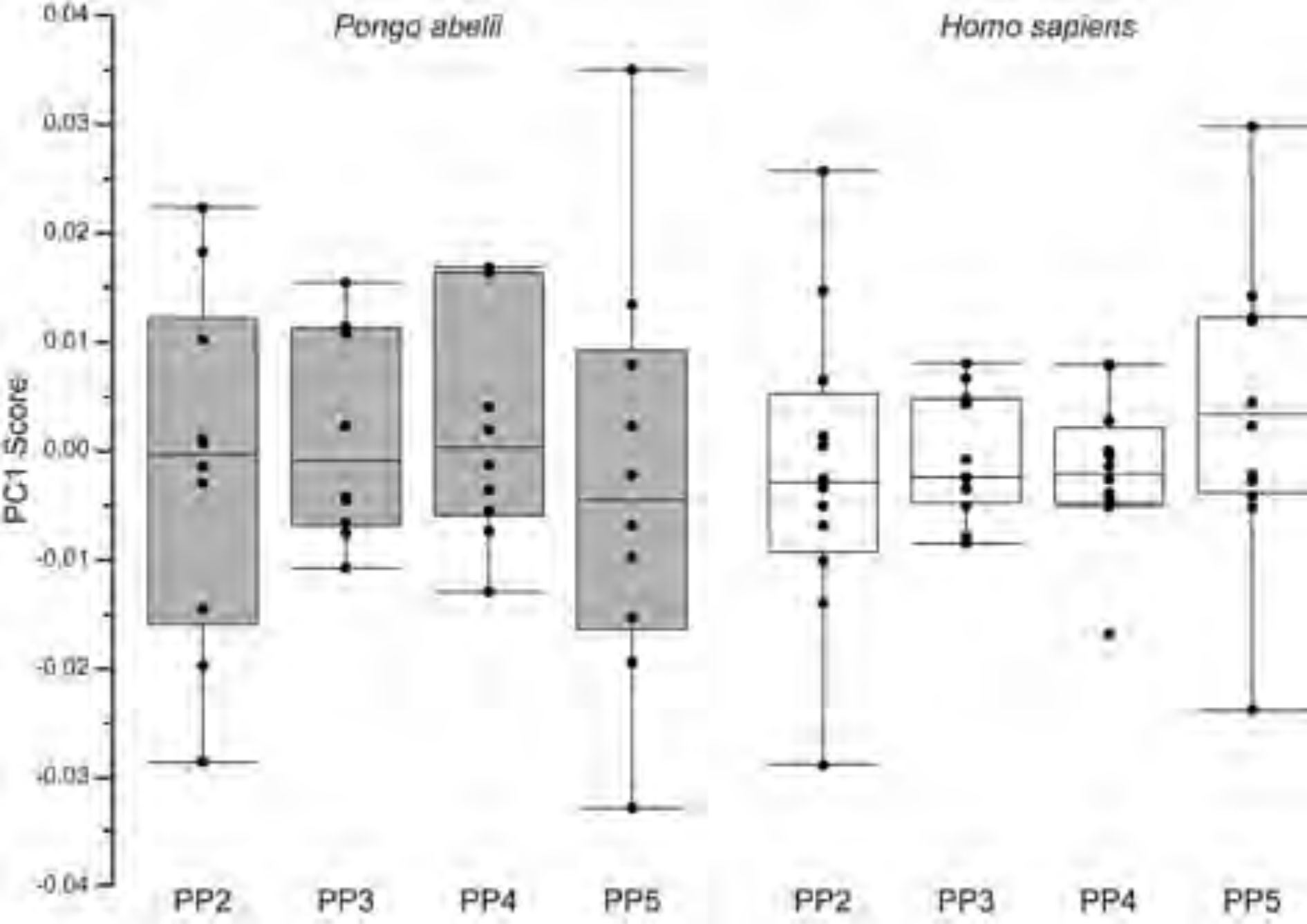
Pongo abelii
Homo sapiens
PC1 Score
0.04
0.03
0.02
0.01
0.00
-0.01
-0.02
-0.03
-0.04
PP2
PP3
PP4
PP5
PP2
PP3
PP4
PP5

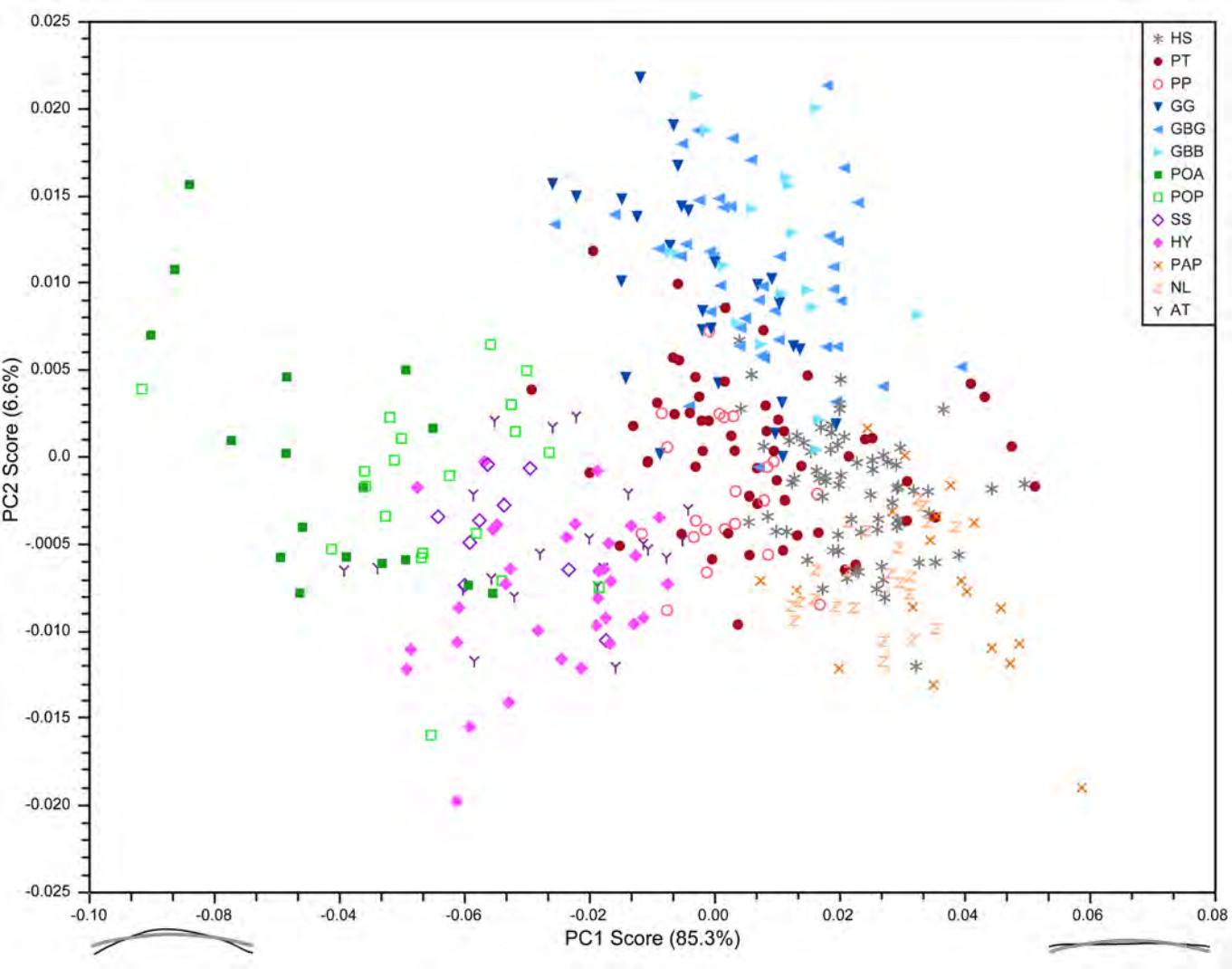
HS
PT
PP
GG
GBG
GBB
POA
POP
SS
HY
PAP
NL
AT
PC2 Score (6.6%)
PC1 Score (85.3%)
0.025
0.020
0.015
0.010
0.005
0
-.0005
-0.010
-0.015
-0.020
-0.025
-0.10
-0.08
-0.04
-0.06
-0.02
0.00
0.02
0.04
0.06
0.08

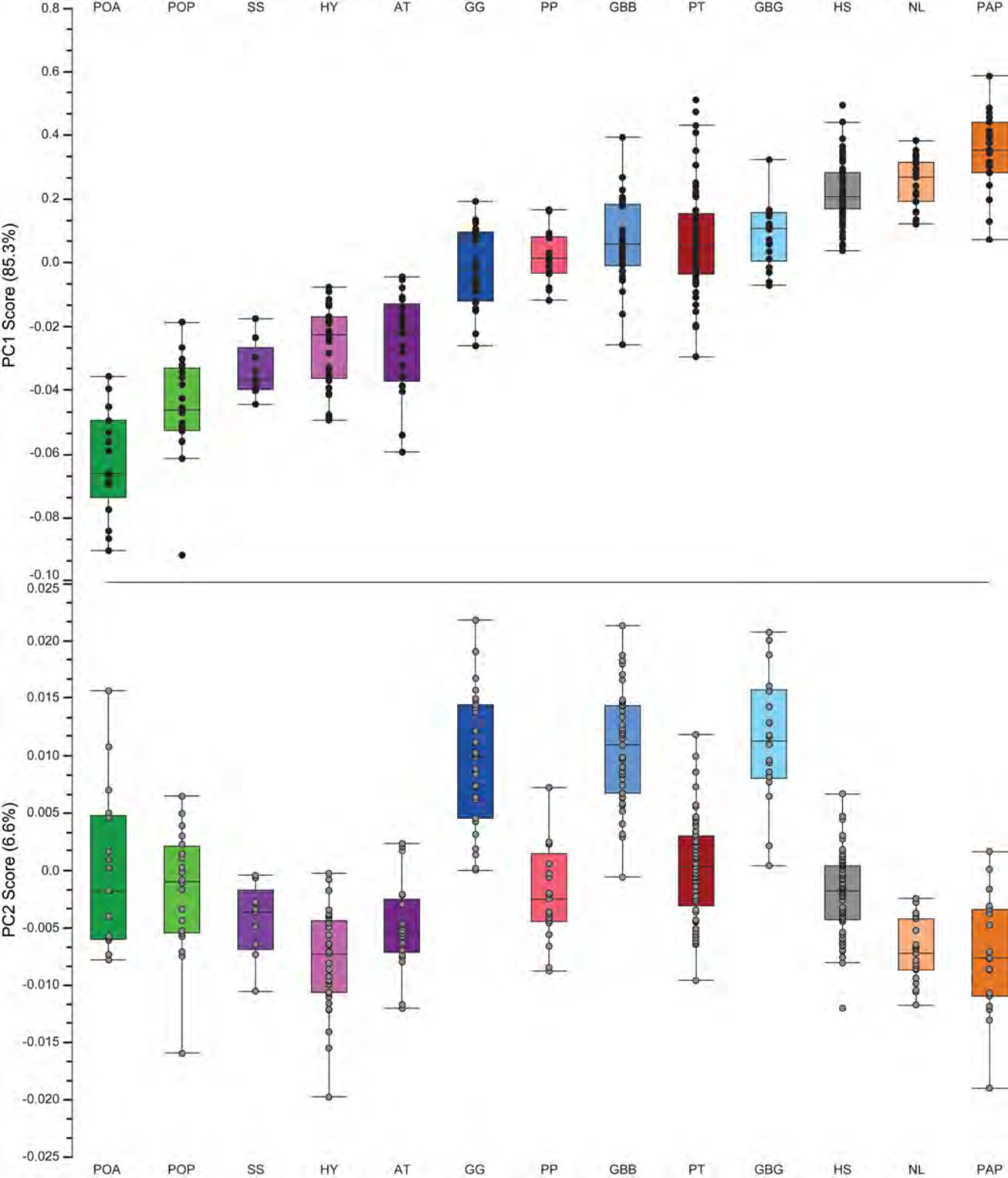
POA
POP
SS
HY
AT
GG
PP
GBB
PT
GBG
HS
NL
PAP
PC1 Score (85.3%)
0.8
0.6
0.4
0.2
0.0
-0.02
-0.04
-0.06
-0.08
-0.10
PC2 Score (6.6%)
0.025
0.020
0.015
0.010
0.005
0.0
-0.005
-0.010
-0.015
-0.020
-0.025

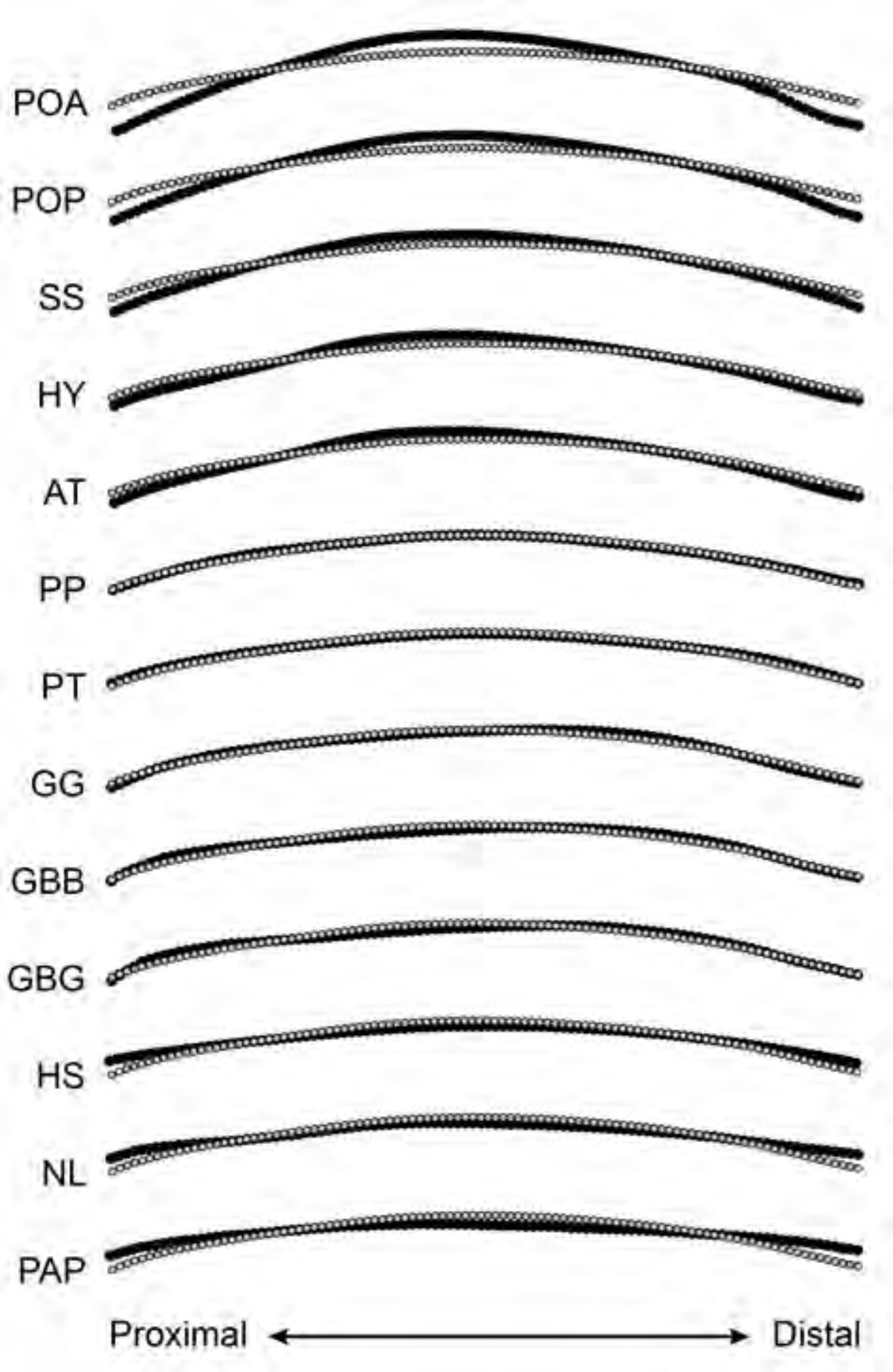
POA
POP
SS
HY
AT
PP
PT
GG
GBB
GBG
HS
NL
PAP
Proximal
Distal

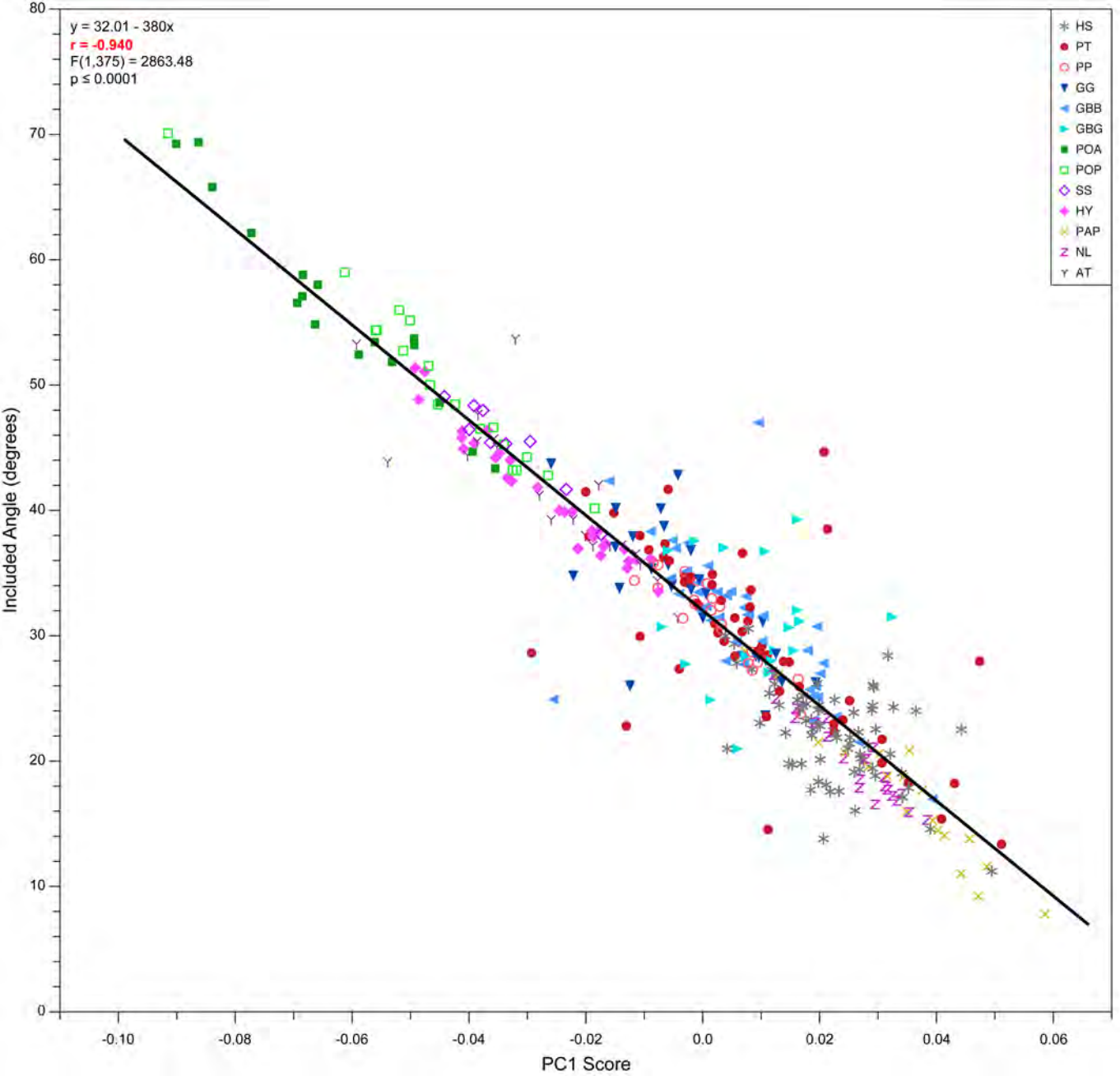
y = 32.01 - 380x
r = -0.940
F(1,375) = 2863.48
p ≤ 0.0001
HS
PT
PP
GG
GBB
GBG
POA
POP
SS
HY
PAP
NL
AT
Included Angle (degrees)
PC1 Score
80
70
60
50
40
30
20
10
0
-0.10
-0.08
-0.06
-0.04
-0.02
0.0
0.02
0.04
0.06

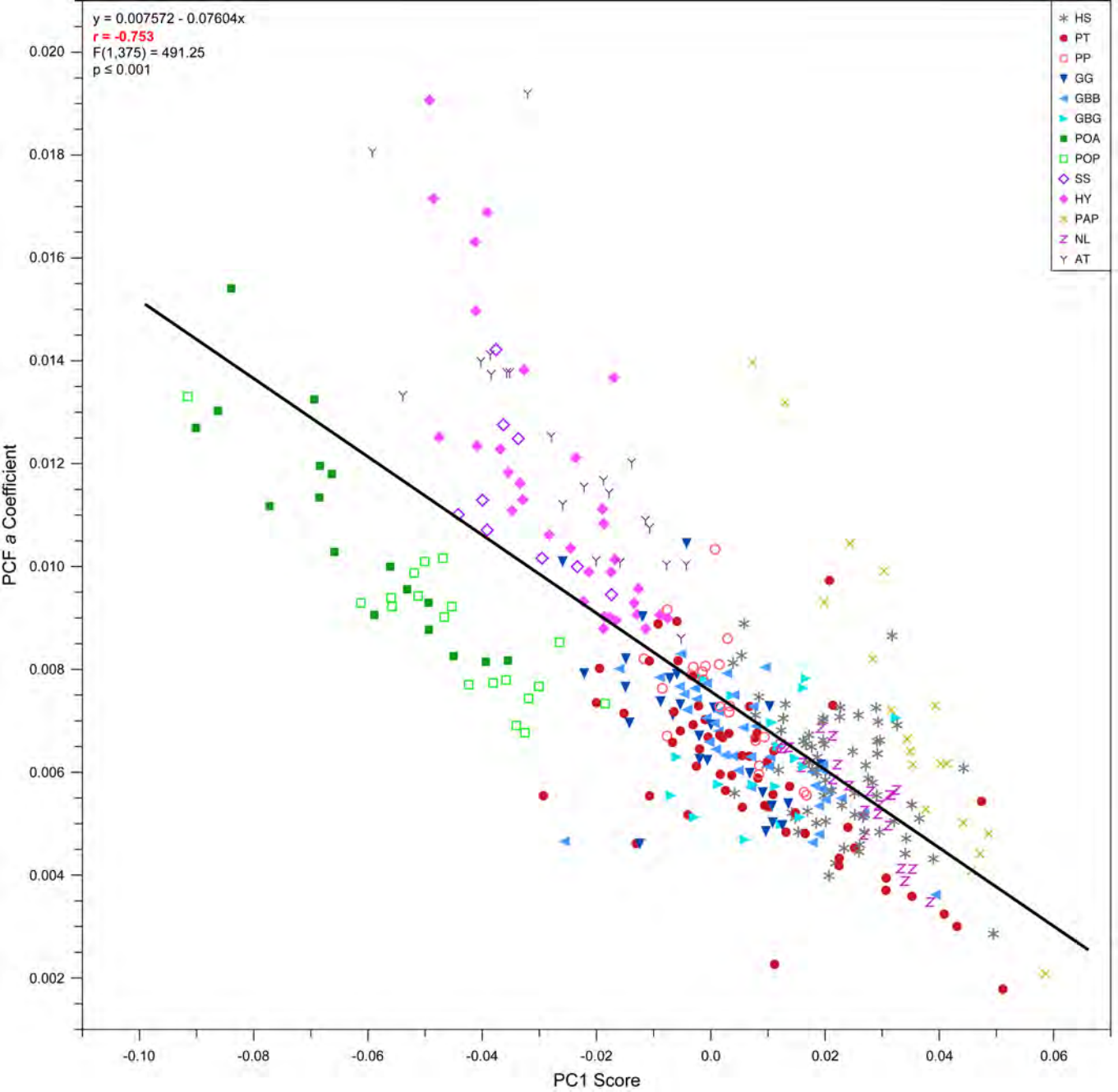
y = 0.007572 - 0.07604x
r = -0.753
F(1,375) = 491.25
p ≤ 0.001
HS
PT
PP
GG
GBB
GBG
POA
POP
SS
HY
PAP
NL
AT
0.020
0.018
0.016
0.014
0.012
0.010
0.008
0.006
0.004
0.002
PCF a Coefficient
-0.10
-0.08
-0.06
-0.04
-0.02
0.0
0.02
0.04
0.06
PC1 Score

SUPPLEMENTAL INFORMATION: ADDITIONAL TEXT & FIGURES

A geometric morphometric approach to investigate primate proximal phalanx diaphysis shape.

Sophie E. Wennemann [1], Kristi L. Lewton [1, 2], Caley M. Orr [3, 4], Sergio Almécija [5, 6, 7], Matthew W. Tocheri [8, 9, 10], William L. Jungers [11, 12], Biren A. Patel [1, 2, *]

[1] Department of Integrative Anatomical Sciences, Keck School of Medicine, University of Southern California, Los Angeles, CA 90033, USA
[2] Human and Evolutionary Biology Section, Department of Biological Sciences, University of Southern California, Los Angeles, CA 90089, USA
[3] Department of Cell and Developmental Biology, University of Colorado School of Medicine, Aurora, CO 80045, USA
[4] Department of Anthropology, University of Colorado Denver, Denver, CO 80217, USA
[5] Division of Anthropology, American Museum of Natural History, Central Park West at 79th Street, New York, NY 10024, USA
[6] New York Consortium in Evolutionary Primatology, New York, NY, USA
[7] Institut Català de Paleontologia Miquel Crusafont, Universitat Autònoma de Barcelona, c/ Columnes s/n, Campus de la UAB, 08193, Cerdanyola del Vallès, Barcelona, Spain
[8] Department of Anthropology, Lakehead University, Thunder Bay, Ontario P7B 5E1, Canada
[9] Human Origins Program, National Museum of Natural History, Smithsonian Institution, Washington DC 20013, USA
[10] Australian Research Council Centre of Excellence for Australian Biodiversity and Heritage, University of Wollongong, Wollongong, New South Wales, 2522, Australia
[11] Department of Anatomical Sciences, Stony Brook University, Stony Brook, NY 11794, USA
[12] Association Vahatra, BP 3972, Antananarivo 101, Madagascar

* Corresponding author: Biren A. Patel, 1333 San Pablo Street, BMT 404, Keck School of Medicine, University of Southern California, Los Angeles CA, 90033, USA; birenpat@usc.edu

1. Adults vs. subadults

As indicated in the main text, the majority of all mPP3 specimens in this study were considered skeletally adult and had fully fused proximal epiphyses. However, in order to augment sample sizes, a handful of non-human sub-adult specimens were also included in this study if the proximal epiphysis was in the process of fusion and could not be manually separated from its diaphysis. The taxa that included skeletally sub-adult specimens were *Pongo abelii* (n=7), *Pongo pygmaeus* (n=1), *Gorilla gorilla* (n=1), *Gorilla beringei beringei* (n=1), *Pan troglodytes* (n=3), *Symphalangus syndactylus* (n=2), *Hylobates* spp. (n=4), and *Ateles* spp. (n=2) (see Table 1 in main text for additional details). For adult specimens, the most biomechanically relevant region of interest of the diaphysis (dROI) was defined between the palmar-most aspect of the proximal palmar tubercles and the inflection point between the distal trochlea and the diaphysis on the palmar side. For sub-adult specimens, the proximal end of the dROI was defined as the point just distal to the zone of epiphyseal fusion which is always just slightly distal to the palmar tubercles. The distal end of the dROI was the same for adults and subadults. Specimens characterized as subadults were combined with adult specimens in all the 2DGM analyses. As seen in the box-and-whiskers plots, PC1 scores of sub-adults for each taxon are within the ranges of variation observed for their adult counterparts (Fig. S1). Therefore, for those taxa studied here, skeletal subadults (as defined here) do not have proximal phalangeal diaphysis shapes that reflect greater or lesser curvature than skeletal adults with fully fused proximal epiphyses. It is important to acknowledge that the current study did not look at shape in very young individuals including infants and juveniles that lack any fusion of the proximal epiphyses (e.g., Richmond, 1998), therefore additional testing and sensitivity analyses would be needed to confirm if the methods implemented in this study can be used on these specimens and combined with older individuals. The same applies for incomplete and broken proximal phalanges which can be of interest to paleoanthropologists given the fragmentary nature of the fossil record (e.g., Deane & Begun, 2008).

Figure S1: Adults vs. subadults. Box-and-whiskers plots of PC1 scores for the 2DGM analysis evaluating manual proximal phalanx diaphysis shape in the comparative sample. Adult specimens (with complete epiphyseal fusion) are shown in solid black circles and subadults (with incomplete and partial epiphyseal plate fusion) are shown in solid red diamonds. Note that

subadult specimens for each taxon have PC1 scores, and thus diaphysis shapes, that are within their respective total adult variation observed here. Horizontal lines within each box illustrate the median of the distribution. Boxes envelop the inter quartile range (50% of values) of the sample distribution, and whiskers encompass the range excluding outliers. Filled circles beyond whiskers indicate outliers. Specimens ordered from left to right based on mean PC1 score. Abbreviations: HS, *Homo sapiens*; PT, *Pan troglodytes*; PP, *Pan paniscus*; GG, *Gorilla gorilla*; GBB, *Gorilla beringei beringei*; GBG; *Gorilla beringei graueri*; POA, *Pongo abelii*; POP, *Pongo pygmaeus*; SS, *Symphalangus syndactylus*; HY, *Hylobates* spp.; PAP, *Papio* spp.; NL, *Nasalis larvatus*; AT, *Ateles* spp. See Table 1 in main text for additional information about the comparative sample.

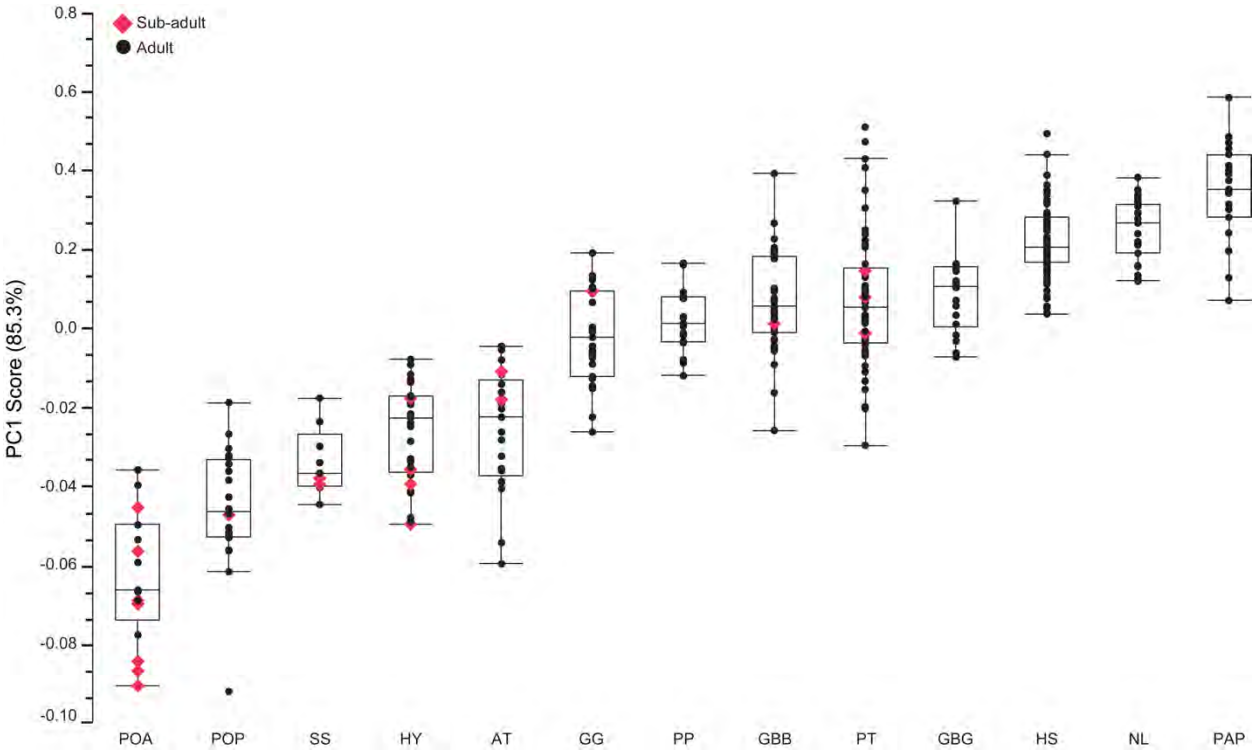

2. Surface mesh triangle count

As noted in the main text, mPP3 surface data derived from a variety of surface scanning and X-ray technologies, as well as researchers, can yield different quality 3D meshes, including different numbers of triangles in the final surface intended for analyses. Ultimately, all our surfaces were either decimated or refined to contain a mesh triangle count of approximately 250,000 triangles. To some readers, this could appear as arbitrary, or possibly as either too high or not enough in number, to ensure accurate results. To assess this issue, we took one orangutan specimen (*Pongo abelii* AMNH-143598) and created 18 variants of its surface mesh ranging from 2,500 to 2,000,000 triangles (Fig. S2A), thereby mimicking outputs from low-resolution laser surface scans to high-resolution μCT scans, respectively. We then performed all the landmark acquisition and 2DGM procedures outlined in the main text on these variants without altering any other parameter or inputs (i.e., same specimen orientation, same dROI dimensions, etc.). The resulting PC1 (31.1% of the variation) and PC2 (22.4% of the variation) scores of each of the 18 variants of the 2DGM analysis were then subjected to a visualization of convergence to assess the relationship with surface mesh triangle count. Among the 18 variants, those with a surface mesh of >100,000 triangles begin to converge in both PC1 and PC2 scores (Fig. S2B and S2C). Based on these observations, we concluded that our 'gold standard' defined as a surface mesh with a count of ~250,000 triangles is sufficiently higher than is necessary, but also without being too excessive.

Figure S2: **Surface mesh triangle count**. A) 3D surface models of the manual proximal phalanx of digit 3 (mPP3) in medial view of a *Pongo abelii* (USNM-143598) with varying numbers of surface mesh triangles (top to bottom: 2,500 triangles; 20,000 triangles; 250,000 triangles; 1,000,000 triangles). Notice that the quality of mesh visually improves after reaching >20,000 triangles. B) Bivariate scatter plot of surface mesh triangle count vs. PC1 score. Notice that variation in PC1 scores begin to stabilize after a model has 100,000 triangles. C) Bivariate scatter plot of surface mesh triangle count vs. PC2 score. Notice that variation in PC2 scores begin to stabilize after a model has 100,000 triangles. The number of surface mesh triangles for all specimens of all taxa ultimately used in this study approximated 250,000 (seen here as the gold diamond for USNM-143598).

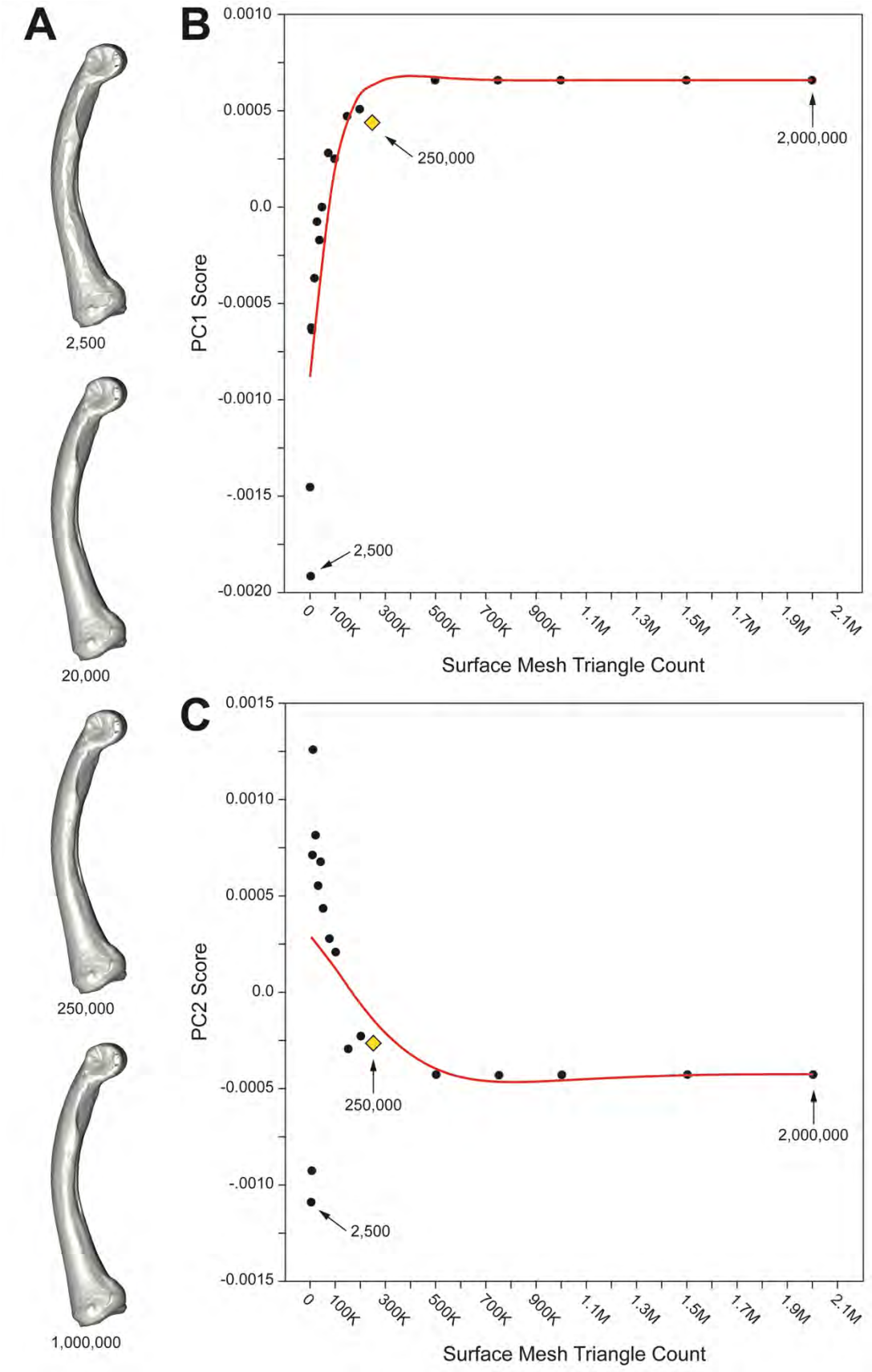
A
2,500
20,000
250,000
1,000,000
B
PC1 Score
0.0010
0.0005
0.0
-0.0005
-0.0010
-.0015
-0.0020
250,000
2,000,000
2,500
0
100K
300K
500K
700K
900K
1.1M
1.3M
1.5M
1.7M
1.9M
2.1M
Surface Mesh Triangle Count
C
PC2 Score
0.0015
0.0010
0.0005
0.0
-0.0005
-.0010
-0.0015
250,000
2,000,000
2,500
0
100K
300K
500K
700K
900K
1.1M
1.3M
1.5M
1.7M
1.9M
2.1M
Surface Mesh Triangle Count

3. Shape variation along PC1 and PC2

Figure S3: Maximum and minimum manual proximal phalanx diaphysis shapes (black filled circles) derived from the Principal Component Analysis conducted on Procrustes coordinates for the comparative sample (see Figure 8 in the main text). Sample mean shapes (gray filled circles) compared to A) maximum PC1 shape, B) minimum PC1 shape, C) maximum PC2 shape, and D) minimum PC2 shape.

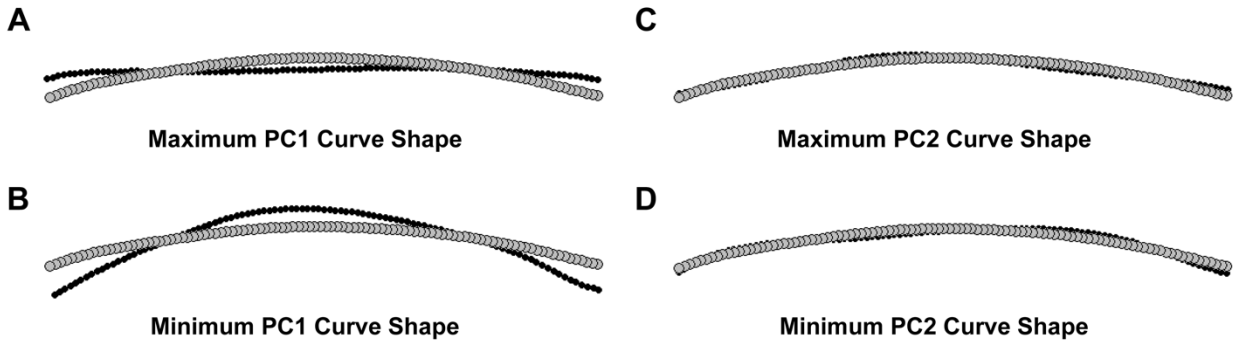

4. Size Correlation

Figure S4. Size Correlation. Bivariate scatter plot of mean natural log (ln) dROI length vs. mean PC1 score evaluating possible size correlation. A) All taxa analysis (n=13) has a significant correlation (r=-0.607; *p*=0.028). B) With *Pongo* and *Papio* removed (n=10) the correlation is not significant (r=0.163; *p*=0.653). Abbreviations: HS, *Homo sapiens*; PT, *Pan troglodytes*; PP, *Pan paniscus*; GG, *Gorilla gorilla*; GBB, *Gorilla beringei beringei*; GBG; *Gorilla beringei graueri*; POA, *Pongo abelii*; POP, *Pongo pygmaeus*; SS, *Symphalangus syndactylus*; HY, *Hylobates* spp.; PAP, *Papio* spp.; NL, *Nasalis larvatus*; AT, *Ateles* spp. See Table 1 for additional information about the comparative sample.

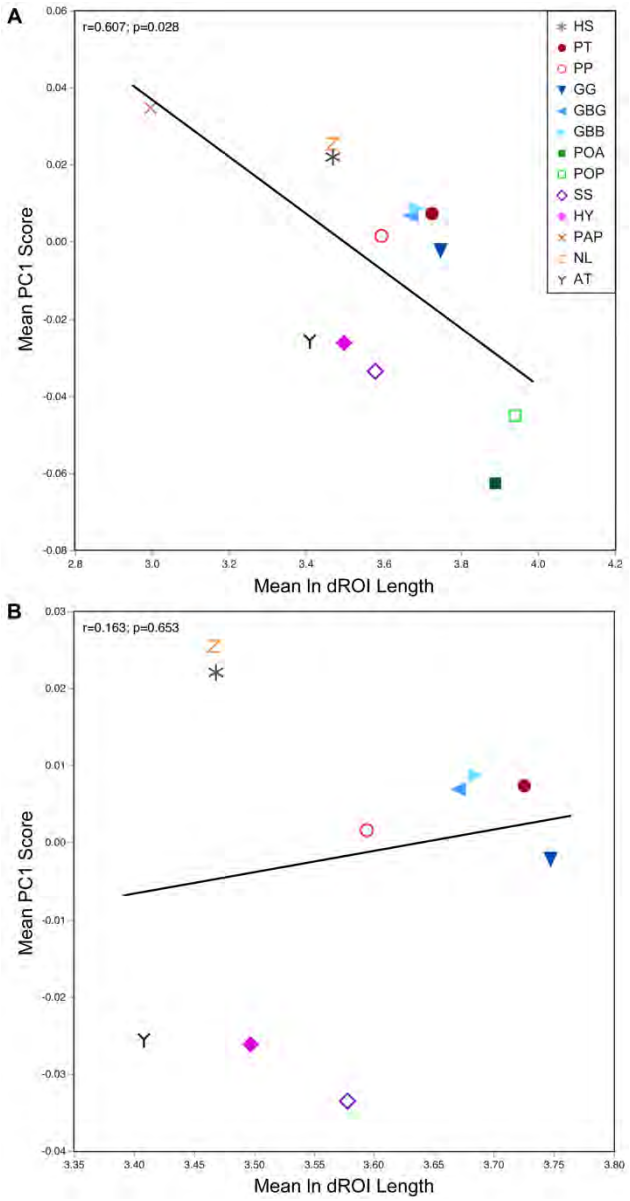

5. Method to calculate IA and *a* from 2DGM landmarks

PC1 scores from the 2DGM analysis of the entire comparative sample of 378 specimens were correlated with each specimen's included angle (IA; measured in degrees) and its second-degree polynomial *a* coefficient. Both IA and *a* were determined from the same set of 2D landmarks of the dROI needed for the 2DGM shape analysis (Fig. S5). Three of the landmarks – proximal [#1], middle [#50], and distal [#100] – were used to calculate IA from overall length (L) and midshaft height (H) following modified calculations presented in Jungers et al. (1997). All 100 landmarks were used to fit a second-degree polynomial to determine the *a* coefficient following Deane, Kremer & Begun (2005). Calculations for both IA and *a* were performed in Excel software. One important difference between Deane, Kremer & Begun's (2005) study and the present one is that the second-degree polynomial was applied to the dorsal surface of the phalanx's diaphysis in the former study whereas the second-order polynomial was applied to the bone's longitudinal proximodistal central axis in present study (compare Fig. S5 below with Fig. 2B in the main text); the approach used here in the present study is more biomechanically appropriate.

Figure S5: Method to calculate IA and *a* from 2DGM landmarks. Methodology to quantify the included angle and the second-degree polynomial *a* coefficient from the 100 2D landmarks used in the 2DGM analysis described in the main text. The included angle and *a* coefficient for each specimen were then correlated with its PC1 score to assess comparability between methods used to assess proximal phalangeal curvature and proximal phalanx diaphysis shape (see also Figures 11 and 12 in the main text; see also Fig. S6).

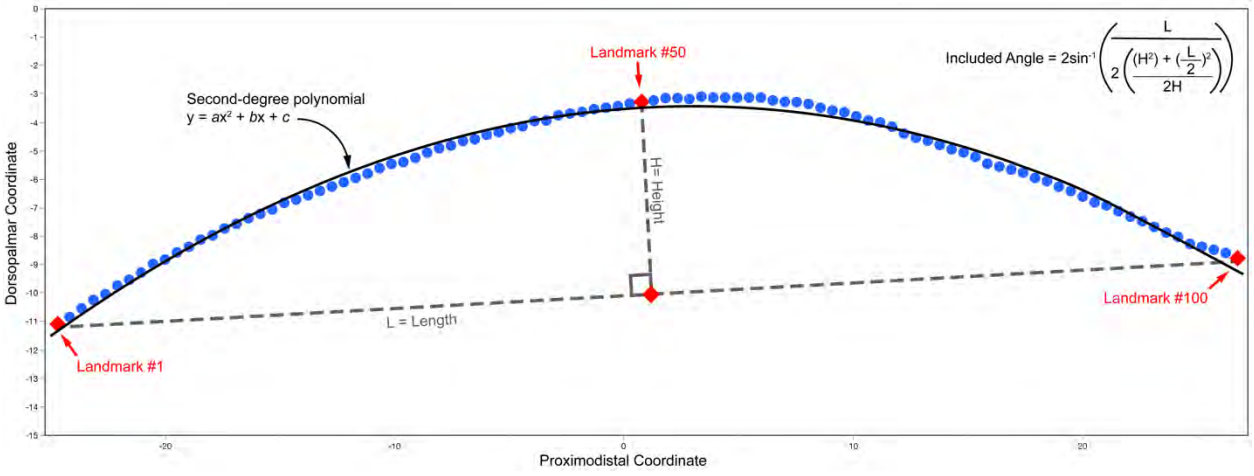

6. 2DGM vs. IA vs. PCF

Figure S6: 2DGM vs. IA vs. PCF. Box-and-whiskers plots of PC1 scores (top, blue), included angles in degrees (middle, red), and PCF *a* coefficients (bottom, black) derived from the same 100 landmark datasets as described in the main text (see also Fig. S5). Note that PC1 scores and included angles do a better job in discriminating between taxa based on habitual locomotor modes, whereas PCF *a* coefficients are only good at distinguishing highly suspensory taxa (i.e., *Pongo*, hylobatids, and *Ateles*) from all other groups. Horizontal lines within each box illustrate the median of the distribution. Boxes envelop the inter quartile range (50% of values) of the sample distribution, and whiskers encompass the range excluding outliers. Filled circles beyond whiskers indicate outliers. Specimens ordered from left to right based on mean PC1 score. Abbreviations: HS, *Homo sapiens*; PT, *Pan troglodytes*; PP, *Pan paniscus*; GG, *Gorilla gorilla*; GBB, *Gorilla beringei beringei*; GBG; *Gorilla beringei graueri*; POA, *Pongo abelii*; POP, *Pongo pygmaeus*; SS, *Symphalangus syndactylus*; HY, *Hylobates* spp.; PAP, *Papio* spp.; NL, *Nasalis larvatus*; AT, *Ateles* spp. See Table 1 in main text for additional information about the comparative sample.

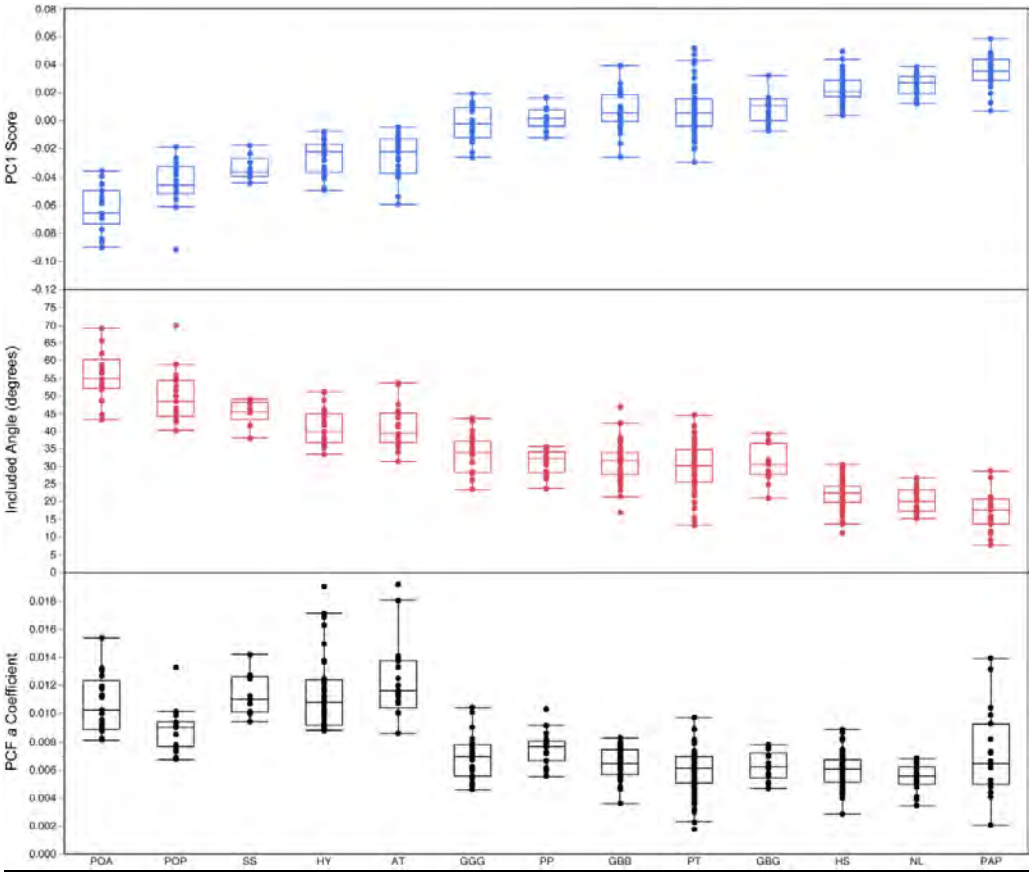

7. R code for 2DGM analysis

```
library(geomorph)

#Read morphologika files
#Morphologika files should be in one folder with the read.multi.morphologika support code available on Github:
https://github.com/EmSherratt/MorphometricSupportCode/blob/master/read.multi.morphologika.R
filelist <- list.files(pattern = "*.txt")
mPP <- read.morphologika(filelist)
dimnames(mPP)[[3]] <- gsub(".txt","",filelist)

#Perform Generalized Procrustes Analysis
mPP.gpa <- gpagen(mPP, PrinAxes=TRUE, max.iter=NULL, Proj=TRUE, print.progress=TRUE)

#Examine outliers
plotOutliers(mPP.gpa$coords)

#Perform Principal Component Analysis & export table of PC scores
PCA <- gm.prcomp(mPP.gpa$coords)
summary(PCA)
write.table(PCA$x, "PCScores.txt", sep="\t")

#Visualize shapes at extremes of principal component axes
ref<-mshape(mPP.gpa$coords)
PC1min <- plotRefToTarget(ref,PCA$shapes$shapes.comp1$min, method="points")
PC1max <- plotRefToTarget(ref,PCA$shapes$shapes.comp1$max, method="points")
PC2min <- plotRefToTarget(ref,PCA$shapes$shapes.comp2$min, method="points")
PC2max <- plotRefToTarget(ref,PCA$shapes$shapes.comp2$max, method="points")
```

8. *Morphologika* Data

Landmark data files in *Morphologika* format for the entire comparative sample of humans, apes, and monkeys (n=378) are available on journal's website to download as Zip file. The Zip file also contains a single .cvs file with specimen classifier information and the "read.multi.morphologika" as noted above in #7.

9. References cited in Supplemental Information

Deane, A. S., Kremer, E. P., & Begun, D. R. (2005). New approach to quantifying anatomical curvatures using high-resolution polynomial curve fitting (HR-PCF). *American Journal of Physical Anthropology*. 128, 630–638. https://doi.org/10.1002/ajpa.20202

Deane, A. S., & Begun, D. R. (2008). Broken fingers: retesting locomotor hypotheses for fossil hominoids using fragmentary proximal phalanges and high-resolution polynomial curve fitting (HR-PCF). *Journal of Human Evolution*. 55, 691–701. https://doi.org/10.1016/j.jhevol.2008.05.005

Jungers, W. L., Godfrey, L. R., Simons, E. L., & Chatrath, P. S. (1997). Phalangeal curvature and positional behavior in extinct sloth lemurs (Primates, Palaeopropithecidae). *Proceedings of the National Academy of Sciences*. 94, 11998–12001. https://doi.org/10.1073/pnas.94.22.11998

Richmond, B. G. (1998). Ontogeny and biomechanics of phalangeal form in primates. Ph.D. Dissertation, State University of New York at Stony Brook, Stony Brook.